**11/24/2003**

# Size-Distributions and Mixtures of Dust and Black Carbon Aerosol in Asian Outflow: Physio-chemistry and Optical Properties

A.D. Clarke[a], Y. Shinozuka[a], V.N. Kapustin[a], S. Howell[a], B. Huebert[a], S. Doherty[b], T.Anderson[b], D. Covert[b], J. Anderson[c], Z. Hua[c], K.G. Moore II[a], C. McNaughton[a], G. Carmichael[d]

[a]-School of Ocean and Earth Science and Technology, University of Hawaii, Manoa
[b]- Department of Atmospheric Sciences, University of Washington
[c]-Arizona State University
[d]- Department of Chemical & Biochemical Engineering, University of Iowa

Keywords: Aerosol, dust, black carbon, soot, absorption, scattering, single scatter albedo, ACE-Asia, TRACE-P

During TRACE-P and ACE-Asia we measured the size distribution of Asian aerosol, their state of mixing, the optical properties of Black Carbon (BC) and other aerosol constituents in combustion and/or dust plumes. Optical particle sizing in association with thermal heating extracted volatile components and resolved sizes for dust and refractory soot that usually dominated light absorption. BC was internally mixed with volatile aerosol in most accumulation mode particles and constituted about 5 to 15% of the mass. These optically effective sizes (OES) constrained the soot and dust size distributions and the dust complex refractive index, **k**, to 0.0006±0.0001. This implies a single scatter albedo, $\varpi$ (550nm), for dust ranging from 0.99+ for $D_p$<1 μm to about 0.90 at $D_p$ = 10 μm and with a size-integrated campaign average near 0.97±0.01. The mass absorption efficiency, MAE, for typical dust distributions was 0.07 ±-0.02$m^2g^{-1}$. South of 25°N less dust and stronger biomass burning signatures resulted in lower values for $\varpi$ of about 0.82 in plumes aloft. Chemically-inferred elemental carbon (EC) was variable relative to BC light absorption ($R^2$ = 0.40) while refractory OES soot volume between 0.1-0.5 μm was highly correlated ($R^2$ = 0.79) with absorption. However, both approaches yield an MAE for BC mixtures of about 7±2 $m^2g^{-1}$ and are higher than calculated MAE values for BC nearer 5 $m^2g^{-1}$. The mass fraction of soot and BC in pollution aerosol increased in the presence of elevated dust due uptake of the volatile components onto the coarse dust. This predictably lowered $\varpi$ for the accumulation mode from 0.84 in typical pollution to about 0.77 in high dust events. A chemical transport model revealed good agreement between model and observed BC absorption for most of SE Asia and in biomass plumes but underestimated BC for combustion sources north of 25°N by a factor of about 3.

## 1. Introduction

The radiative properties of atmospheric aerosol depend upon the size and nature of the mixing of these absorbers with other common atmospheric aerosol such as sulfates, ammonium, nitrates, organic carbon and water. These mixtures range between internal (multiple components within a particle) and external (different components in different particles). Because many of the components are hygroscopic and take up water as a function of relative humidity (RH) then the nature of the soluble and insoluble components of the mixtures determine the size, refractive index and optical properties under ambient RH conditions. Hence, efforts that include the modeling of aerosol radiative properties or the retrieval of aerosol properties from remote sensing and optical measurements need to properly account for these size-dependent properties.

It is well known that the light absorbing BC mass is generally found in the sub-micrometer (hereafter called sub-μ) sizes while most dust mass is in super-micrometer sizes. BC has a strong light absorption per unit mass (or mass absorption efficiency - MAE) and sub-micrometer refractory dust has much lower MAE. The complex refractive index of ambient atmospheric soot, BC and dust are essential parameters for modeling their light absorption but they remain poorly characterized. Soot can be a complex mix of components that include absorbing BC. The influence of size, morphology, aggregation, composition, refractive index and other characteristics influencing BC optical properties are carefully examined in a paper by *Fuller, Malm and Kriedenweis* [1999], hereafter referred to as FMK.

Dust optical properties are uncertain for different reasons. In the aerosol phase the particles have irregular shapes difficult to model [*Kalashnikova and Sokolik*, 2002; *Mishchenko et al.*, 1997] and may have weathered surfaces that differ chemically from the parent material or may be coated with other non-absorbing or absorbing components. *Sokolik and Toon* [1999] have revised earlier estimates of dust complex refractive index downward and suggest a **k** value for dust with 1% hematite lies somewhere near 0.001 at a wavelength of 0.55 um. *Kalashnikova and Sokolik* [2002] use this value in their model and report a range of single scatter albedo between 0.969 and 0.978 depending on the dust shape for an assumed lognormal distribution with a number median diameter of 1 um. These recent simulated values for single scatter albedo are in good agreement with in-situ observations [*Anderson*, 2003; *Clarke and Charlson*, 1985; *Clarke et al.*, 2001; *Kaufman et al.*, 2001] and the observations discussed here.

In this paper we will focus attention upon the measured size-resolved light-absorbing properties of dust and BC. These will be discussed in conjunction with characteristics of the accumulation and coarse mode aerosol, the soot component of the aerosol and concurrent elemental carbon, EC, measurements. Hence, it is important to clarify these terms in this paper. BC is used here as the light absorbing component of the soot aerosol. We use the word "soot" here to represent the combination of BC with other species emitted near the combustions source that might be mixed with it such as OC, or pyrolized and unburned fuel etc. At times "soot/BC" will be used to emphasize this link. In this study flyash is considered separate from soot since it is generally observed as particles with a distinct and separate morphology [*Shi et al.*, 2003]. Because most of our samples were hours to days away from the combustion source this evaluation reflects aged soot emissions often associated with other species that largely comprise what we refer to as the sub-μ accumulation mode. The term EC is retained for the operationally defined carbon mass concentration inferred from the evolution of $CO_2$ detected upon sample filter combustion [*Huebert et al.*, 2003].

During the spring of 2001 we participated in two aircraft experiments as part of NASA TRACE-P [*Jacob et al.*, 2003] and ACE-Asia [*Huebert et al.*, 2003] studying the microphysical and optical properties of Asian aerosol advected over the North Pacific. These sequential experiments with nearly identical instrumentation provided a unique opportunity to investigate outflow from East Asia between 5N and 50N during the same season. The TRACE-P experiment (Feb. 24,2001-April 10, 2001) was initially based in Hong Kong and after March 17 was based in Yakota, Japan. ACE-Asia flights were based out of Iwakuni, Japan from March 31$^{st}$ to May 4$^{th}$ 2001. All ACE-Asia measurements were made using the Low Turbulence Inlet (LTI) and the TRACE-P measurements employed our NASA-UH shrouded solid diffusor inlet, both of which were evaluated in the PELTI experiment [*Huebert*, 2003]. The last two TRACE-P flights were flown in conjunction with the first two ACE-Asia flights allowing us to quantitatively compare instrumentation on both aircraft [*Moore et al.*, submitted 2003]. Differences were small and do not affect the analysis or conclusions in this paper.

## 2. Instrumentation

The aircraft aerosol data discussed here includes measurements of number, size, composition, and optical properties along with related measurements of gas phase species. These include:

- Aerosol size distributions obtained from a laser optical particle counter (OPC a modified LAS-X, PMS, Boulder, Co.). Optically effective size (OES) distributions were obtained between diameters of 0.1 and 14 μm based upon spherical calibration particles with a refractive index of 1.588 up to 2 μm and 1.54 above that. Because these OES distributions include effects of shape they are most useful for modeling optical properties. Adjustments to aerodynamic or geometric sizes require additional information on shape, density and refractive index.
- The OPC was operated with thermo-optic aerosol discriminator (TOAD) in order to infer size-dependent volatility by cycling aerosol through heaters at 150°C and at 300°C (ACE-Asia) or 350°C (TRACE-P). Heating to 150°C is designed to drive off low temperature volatiles (sulfuric acid and some nitrates and OC) while heating to 300+°C is designed to volatilize ammonium sulfate [*Clarke*, 1991]. The residual "refractory" aerosol includes most light-absorbing soot (and Black Carbon -BC) below about 1μm while the larger refractory component is generally dust or occasionally sea-salt.
- A radial differential mobility analyzer (DMA) provided additional size information between 0.007 μm and 0.15 μm . Dual DMA's were also operated periodically in Tandem DMA mode (TDMA) with similar thermal analysis. One DMA selects a specific size for thermal conditioning before scanning with a second DMA. DMA samples were collected over 20s and held in a lagged aerosol grab (LAG) chamber [*Clarke et al.*, 1998] for subsequent DMA analysis.
- Total aerosol number concentrations were measured at 1Hz with an Ultrafine Condensation Nuclei counter (UCN; TSI 3025) and with two CN counters (TSI 3760 or TSI 3010) both operated at 40 and 360°C. CN counters operating at 300°+ reveal the refractory number concentration of the aerosol that often provides a rapid indication of air mass character not always evident in the total concentration [*Clarke et al.*, 1997]

- Two 3-wavelength TSI 3563 nephelometers were used on the C-130 during ACE-Asia to simultaneously measure coarse and fine aerosol light-scattering. The latter was measured using a 1 μm aerodynamic impactor [*Anderson*, 2003] TRACE-P employed a similar TSI nephelometer but with an identical impactor cycled sequentially to alternately measure total and sub-μ light scattering.
- Light absorption was measured with a Particle Soot Absorption Photometers (PSAP, Radiance Research) on both aircraft with and without a 1μm aerodynamic impactor. Again, total and sub-μ measurements were continuous on the C-130 and measured alternately on the P3-B. Corrections for artifact absorption due to scattering were applied after [*Bond et al.*, 1999]. In conjunction with the light-scattering this also established coarse and fine aerosol single scatter albedo [*Anderson*, 2003]. On TRACE the PSAP operated at about 4-5 lpm resulting in impaction losses of about 50% for 4 μm particles while on ACE it was operated at 1 lpm. Our post experiment tests found this to result in impaction losses of 50% at 12.5 μm. The higher flow rate made coarse particle losses potentially greater on TRACE, but this effect was seldom significant because few dust events encountered.[1999]
- A Particle in Liquid Sample (PILS) [*Orsini et al.*, 2003; *Weber et al.*, 2001] employs a steam saturator followed by impaction of wet aerosol for collection and measurement of major ions every few minutes using ion chromatography. The PILS provides soluble [eg. sulfate, nitrate] and refractory species that influence refractive index and hygroscopic behavior with about 4 min resolution.
- Elemental Carbon (EC) and Organic Carbon (OC) are operationally defined measures of BC and OC based upon the thermal evolution of $CO_2$ and were measured on samples collected from the ACE-Asia aircraft using the Sunset Labs instrument. [*Huebert et al.*, 2003] with estimated uncertainty of 30% for this data.

Thermal heating of the dried aerosol (RH<40%) prior to analysis by both the DMA and OPC was an important feature of our measurements on both experiments. Primary emissions of refractory particles are often present in both fine (soot, flyash) and coarse sizes (sea-salt, dust) and are thermally separable from most volatile sulfates, nitrates and OC. In remote oceanic regions we have previously shown how aerosol volatility can be linked to the volatile sulfate aerosol and its relative neutralization by ammonia [*Clarke*, 1991]. In spite of the greater complexity of the Asian aerosol chemistry we have been able to quantitatively relate our observed volatile volume to soluble ions obtained from the PILS technique between diameters of 0.1 and 1.2 μm. These sizes contain most of the volatile mass and the soluble mass. This study yielded a regression leg average OPC and PILS mass with a slope of 1.05 and an $R^2$ of 0.78 and supports our use of volatility as an indicator for aerosol chemistry. The details of this comparison are the subject of a separate paper that focuses upon the humidity response of the Asian aerosol [*Howell et al.*, submitted 2004].

## 3. The TRACE-P and ACE-Asia experiments

Comparison of data sets from different experiments can often be problematic due to different instrumentation or sampling approaches. Consequently, deliberate side-by-side flights were made for the TRACE-P P3B and the ACE-Asia C-130 during the few days these two

experiments overlapped. In spite of differences in inlet types aerosol sizing and optical properties agreed within instrument uncertainty at all altitudes [*Moore et al.*, submitted 2003] and provides confidence that these and the related optical measurements discussed here are comparable and can be combined.

Figure 1 shows mission-average vertical profiles for scattering, absorption and single scatter albedo for both experiments. Aerosol absorption is present throughout both study regions in the lowest 3km but concentrations vary with sources from regional scales, urban center scales and down to plume scales of several km. TRACE-P flight data has been separated into data collected south and north of 25°N in view of chemical and meteorological differences evident for these regions [*Jacob et al.*, 2003]. The 19 ACE-Asia flights were north of 25°N (Figure 1, bottom panels) and are compared to the 5 TRACE-P flights north of 25°N (top panels) even though the number of flights, time periods and meteorological conditions differed. The average TRACE-P data south of 25°N (middle panels) suggest a dominant scattering and absorbing layer below 1km with a deeper 1 to 4 km layer above characterized by moderate scattering but high absorption with transitions to lower and more typical values for both above 4km. This layer aloft also has chemical signatures associated with biomass burning [*Ma et al.*, 2003]. The associated profile for $\varpi$ shows highest values near 0.92 at the surface that drop to about 0.8 near 2 km. Variation in $\varpi$ around this value continues up to 6km altitude.

The data north of 25°N from both TRACE-P (top panels) and ACE-Asia (lower panels) reveal similar vertical profiles that differ from the data south of 25N. High scattering and absorption values below 1 km trends to lower values aloft. North of 25°N $\varpi$ has values near 0.92 at the surface but increases with altitude to values near 0.95 at 6 km. As discussed below, this increase is largely due to the presence of dust aerosol [*Anderson*, 2003] and the greater frequency of the dust events during ACE-Asia contribute to the higher and more stable average scattering and absorption aloft for this data. Note that average near-surface properties for all 3 examples are similar and show $\varpi$ near $0.925 \pm 0.015$ (circled) in contrast to the variability evident aloft. These surface values provide a poor representation of the column properties in both regions and emphasize the importance of aircraft data in establishing aerosol and optical properties over the atmospheric column. The indicated standard deviation for this average profile reveals the large variability in the aerosol. These variations below the inversion were often on the order of 10's of percent over vertical scales of 100m or less and horizontally over scales of a few kilometers.

### 3.1 Observed Morphology of Dust and Soot

It is important to keep in mind the physical properties of the aerosol when considering its optical effects. Figure 2 illustrates actual scanning electron micrographs of aerosol types sampled during Flight 13 of ACE-Asia in the Yellow Sea at altitudes of 5,500 m, 700 m and 250 m. The high altitude samples shows generally sharp-edged dust aerosol with some occasional soot particles but the size of soot clusters, their abundance and attachment to dust surfaces increases at low altitudes. Most isolated soot clusters and round "balls" have a graphitic nature (open circles) and were originally coated with volatiles. Other features are identified in the figure. Note that thermal heating of the particles by the high beam current in the SEM during this analysis drives off many volatile species such as sulfate and low temperature OC [*Li et al.*, 2003] leaving the more refractory components shown here. We presume that the dust and soot

particles remaining in these images are similar to those detected in the 300°C OPC OES distributions. The complexity of these mixtures and shapes raise serious questions regarding what is meant by the size of the aerosol since diameters that represent the actual geometric, aerodynamic, optical and effective mass of these particles are likely to be quite different. Hence, we emphasize here the value of optically effective sizes in the interpretation and calculation of aerosol optical properties.

### 3.2 Size Distributions and Volatility

As mentioned earlier, we discuss here the optically effective sizes based upon scattering properties detected by the OPC. These are most useful for regeneration of optical properties via Mie scattering but physical sizes may be quite different. Variability in aerosol optical properties are also related to size dependent variations in composition that are also linked to aerosol volatility. Several examples of OPC thermally-resolved OES distribution data from Flight 13 of ACE-Asia are shown in Figure 3 for diameters between 0.1 and 10 μm. This size range generally encompasses most aerosol mass that influences aerosol radiative effects at visible wavelengths. Each case is an average of several distributions accumulated under similar conditions so that volatility is well characterized and not a result of concentration variations over a single 90 sec measurement period. Data are presented both in a logarithmic format to expose the full range of concentrations and as linear volume distributions (where the area under each curve is proportional to volume) in order to better reveal relative contributions.

This flight was selected because it included very high dust concentrations mixed with a range of soot concentrations. The top row illustrates a moderate dust event associated with low measured sub-μ light absorption and little volatility between 150°C and 300°C between 0.1 and 0.5 μm. Some nitrates or volatile OC can possibly contribute to components volatile at 300°C but sulfate is a major constituent [*Weber et al.*, 2003]. The refractory dust is shown as a linear volume distribution (area under plot proportional to volume) in the top panel corresponding to about 125 μg $m^{-3}$ but the volatile component is no longer resolvable for this mode.

The middle row in Figure 3 illustrates a higher dust concentration on the order of 1,000 μg $m^{-3}$ mixed with more pollution aerosol and the volatile accumulation mode volume corresponds to about 5 μg $m^{-3}$. This and the refractory (300°C) component are an order of magnitude larger than the upper row but this is not evident on the linear plot due to the high dust concentration. Note that the peak diameter for dust volume shifts to larger sizes for the highest dust case (middle row). The bottom row is a low-dust case associated with a moderate sub-μ light absorption coefficient and moderate volatile component (typical of most TRACE-P data). The amount of volatile accumulation mode corresponds to a mass of about 20 μg $m^{-3}$ (about 4 times the previous case) while the coarse particle dust is only about 50 μg $m^{-3}$ (less than 5% of the previous case). Both modes are well resolved on the linear volume plot (right panel). The heated size distributions reveal most volatility is present for sizes below about 0.6 μm but, unlike the previous two cases, a significant fraction of the coarse mode volume is evident as volatile coatings on the coarse dust aerosol. The apparent differences in volatility for the largest sizes above 5 μm are not statistically significant because of low count statistics.. Note that the leftmost panel shows that the refractory mode present between 0.1 and 0.6 μm is much more pronounced than for the very high dust case and the volume peak on the linear scale stands out

clearly relative to the dust. This demonstrates that the sub-μ refractory mode is related to the accumulation mode pollution component and not the dust distribution.

### 3.3 State of mixing in the accumulation mode and smaller sizes.

The refractory soot and dust discussed above are the primary absorbing aerosol. However, the volatile species have a large influence on the scattering and the state of mixing of the aerosol (internal or external) and are important for proper understanding of overall aerosol optical effects. Mixing state can often be inferred from size-resolved volatility. If mass changes upon heating but the integral number do not then the volatile component must be internally mixed with the refractory component. If both number and mass change then some or all particles may be externally mixed depending upon the change in the size distribution. Hence, we use measurements from both the OPC (Fig. 3) and DMA to resolve changes upon heating for both volume and number over the size ranges of interest.

Although most aerosol volume and optical properties present in diameters above 0.1 μm are resolved by the OPC, the ambient number distribution generally contains many particles smaller than this diameter. In order to better understand what controls the total particle number it valuable to resolve the complete size distributions of both total and refractory aerosol. Hence, we have extended our volatility techniques down to 0.01 μm diameter through use of our DMA and TandemDMA (TDMA) instrumentation. Figure 4 shows examples of DMA, TDMA and OPC size distributions from TRACE-P for representative cases of biomass burning and pollution. At 3 km over Hong Kong we encountered a typical aged biomass aerosol plume (Fig 4a) with a moderately high concentration. At 350°C the mode shifts to smaller diameters but preserves a clear mono-modal shape with about 80% of the total original number remaining and 40% remaining at sizes above 0.1 μm. A similar plot for an urban sample (Fig. 4d) shows a greater shift upon heating and about 60% of the total number remaining but only 20% remaining with sizes larger than 0.1 μm.

The changes indicated in the overall DMA distributions are confirmed when TDMA heated scans are done on sizes selected near 0.1 μm. In the biomass example about 93% become smaller upon heating to 350°C with only about 3% remaining near the original size. The latter may be externally mixed or associated with very little volatile material. A similar example for the urban sources shows about 5% of the total number remains in the selected size range after heating. However, both the biomass and urban distributions reveal that over 90% of the sub-μ volume is lost upon heating to 350°C. The TDMA biomass example exhibits a shift in size that preserves a nearly mono-modal shape compared to the urban case that shows a broader distribution after heating also evident in the full DMA distributions. A large change in mass for a small change in number indicates an aerosol that is primarily internally mixed. In all cases, most aerosol present in the accumulation mode are internally mixed with a refractory component. Similar differences in biomass vs. urban measurements of refractory distributions were measured over the Indian Ocean and off the coast of South America. These observations all indicate larger sizes with narrower refractory (presumed to be soot/BC) distributions in biomass plumes compared to broader distributions in urban plumes. The greater range of refractory sizes for the urban cases and may reflect the multiplicity of diverse combustion sources compared to biomass sources.

### 3.4 Separating out Refractory Dust and BC

In Figure 5 we generalize our OES distributions for the entire ACE-Asia data set at times when dust concentrations exceeded about 40 μg $m^{-3}$ in order to explore characteristics of the dust mode and the refractory soot (BC) mode. Coarse particle concentrations below this value can be common in polluted air even when wind-driven dust is not present. These data represent 10 min averages for all refractory OES distributions. The top panel reveals several distinctive features. Sizes below about 0.6 μm show variability over about two orders of magnitude. Between 0.6 μm and 2.0 μm most distributions have similar slopes and vary within about one order of magnitude. The curves diverge more at larger sizes, approaching 3 orders of magnitude at the largest sizes. Data from three legs flown on Flight 13 at 5,500 m (blue), 700 m (red) and 250 m (green) are highlighted since these will be used to illustrate the roles of soot and dust in various discussions that follow. These three sequential legs range from the highest to relatively low dust cases and moderate to lowest soot cases and span the range of aerosol mixes observed during ACE-Asia.

The relative invariance of the slope of the dust mode below 2 μm suggests that the shape of the typical dust distribution might be approximated such that the refractory dust and soot modes could be separately resolved. It was found that consistent results were obtained by normalizing refractory distributions at diameters between about 0.65 to 1.2 μm. Because 0.75 μm OES is about the same as the 1 μm aerodynamic size cut (assuming a density of 2 μg $m^{-3}$) used for various size segregating impactors on ACE-Asia, including the nephelometer [*Anderson*, 2003], we elected to use this diameter for normalization. The greater variability at the largest dust sizes is a result of the sensitivity of these sizes to production and removal processes. Sizes near one micrometer are resistant to removal processes and change less over time and distance from source [*Schütz*, 1980]. Variability in the refractory accumulation mode is driven largely by soot/BC, as will be demonstrated in section 3.6.

After normalization the variation in the refractory distribution (middle panel in Figure 5) is greatly reduced up to about 3 μm diameter while the soot mode retains a spread over about 2 orders of magnitude. The flight 13 legs at 250 m and 700 m now fall on top of each other at the larger sizes while the leg at 5,500 m bounds the lower range of dust cases included here and the lowest of the soot cases. Although the soot mode for this case is small, both direct measurements and optical properties indicate that soot absorption is present (see section 3.7 below). As a result of these observations we have also indicated our so-called "reference" dust distribution for the high dust case that decreases rapidly at OES below 0.5 μm. The refractory volume distribution below 0.75 μm ($V_{ref<75}$) after subtracting our "reference" dust distribution is used to represent the refractory soot and BC component. This approach assumes that the refractory soot is confined to sizes below 0.75 μm but we will demonstrate that this assumption is not always true later in the paper.

The bottom panel in Figure 5 shows the normalized refractory OES number distributions for the 250 m leg along with our reference dust distribution (RefDust) on Flight 13. The shape of the reference dust mode suggested a need for one soot and three lognormal dust modes. Three dust modes have also been identified by other investigators and two of these are included in Table 1. Our modes were established by recognizing the stability of the dust mode near 1 μm and our need to obtain a careful fit to the lower tail of that mode (Dust 1) in order to properly extract the soot mode. Actual fitting was carried out using the area distributions which resolved

a peak in the larger dust mode usually between 5 and 9 μm. We also recognized that our coarse particle mode (Dust 3) was poorly constrained at diameters above about 12 μm so we used a recently determined Dust 3 fit [*Alfaro et al.*, 1998] for Saharan dust. The dust 1 fit was optimized by constraining the mode diameter to be larger than our normalization diameter of 0.75 μm and the standard deviation to be larger than 1.3 while minimizing differences between model and measured area, volume and number distributions in the vicinity of the fit. The mode diameter and standard deviation of the second dust mode, Dust 2, was then allowed to vary until it also minimized differences between measured and model distributions for our normalized high dust cases.

Once these lognormal modes were established, we applied an optimizing technique to adjust the mode amplitudes to best fit our dust OPC optically effective sizes. These three dust modes are compared to three mode fits recently published by [*Alfaro et al.*, 1998] and earlier frequently used fits described by [*d'Almieda*, 1987] in Table 1. Our dust distributions represent those measured on the order of 1,000 km or so from source regions and we might expect the larger 3rd dust mode to be more variable closer to sources. The steep fall off in RefDust volume on this log-log plot below about 1 μm and the more gradual increase to a maximum near 10 μm is also consistent with results fromthe Sahara [*Schütz*, 1980].

Table 1. Lognormal fit parameters to the refractory number distributions shown in Figure 5c. $D_{pi}$ is the geometric mean or median diameter and $\sigma_i$ is the geometric standard deviation as defined in [*Seinfeld and Pandis*, 1998].

| Lognormal Mode | Soot | Dust 1 | Dust 2 | Dust 3 |
|---|---|---|---|---|
| ***This study*** | | | | |
| **MMD [μm]** | **0.27** | **1.06** | **5.51** | **14.2** |
| **Standard deviation** | **1.59** | **1.46** | **1.85** | **1.5** |
| ***D'Almeida* [1987]** | | | | |
| **MMD [μm]** | | **0.83** | **4.82** | **19.36** |
| **Standard deviation** | | **2.10** | **1.90** | **1.60** |
| ***Alfaro* [1998]** | | | | |
| **MMD [μm]** | | **1.5** | **6.7** | **14.2** |
| **Standard deviation** | | **1.7** | **1.6** | **1.5** |

### 3.5 Refractory aerosol and absorption

Apart from obtaining OES fits suitable for modeling the optical properties of the Asian dust distributions, our primary objective in fitting the smaller tail of the dust mode is to better resolve the size distributions of the absorbing soot/BC mode. To demonstrate this capability we plot both the integral refractory volume distribution below 0.75 μm OES ($V_{ref<75}$) against the measured sub-μ PSAP absorption in Figures 6a. In figure 6 b we plot this volume only with the dust component subtracted ($V_{ref<75\ -Dust}$). Both figures are color coded by the total coarse dust volume. For clarity, about 5% of the ACE-Asia data (mostly some low altitude legs over Yellow Sea) has been removed for cases of unusually high sub-μ fly-ash with high sub-μ refractory volume (see Fig 7 discussion below).

Figure 6a shows that for a given value of sub-μ PSAP absorption the values of $V_{ref<75}$ are highest when coarse dust concentrations are highest (red points). This reflects the increasing contribution of sub-μ dust with low sub-μ absorption to $V_{ref<75}$ as dust concentrations increase. The slope of the line (0.16) through the lower limit of data points for very low dust concentrations below 50 $\mu m^3 cm^{-3}$ (blue points) identifies the strong relationship between $V_{ref<75}$ and light absorption due to absorption by soot for low dust. If our reference dust distribution is representative of Asian dust and if our scheme for extracting the sub-μ dust volume from $V_{ref<75}$ is appropriate then we expect a similar strong relationship between the sub-μ absorption and our sub-μ refractory volume when the sub-μ dust component is removed ($V_{ref<75 -Dust}$). This is clearly evident in Figure 6b where virtually all this data collapse down from a slope of 0.27 to a similar slope of 0.14 when our reference dust is subtracted. If our dust subtraction were too large then $V_{ref<75 -Dust}$ values would be consistently low and show up as data points well below other non-dust (blue) cases. Conversely, if the dust subtraction were too little the data would not have been collapsed as effectively. Hence, our fit to the sub-μ refractory dust tail must be quite good. Exceptions are evident in the deep red data points when dust concentrations approach 400 $\mu m^3 cm^{-3}$ (ca. 1000 $\mu g\ m^{-3}$). At these dust concentrations the extracted soot volume fraction is well below 1% of the dust volume. Consequently, as long as the refractory soot volume exceeds 1% of the dust volume this approach defines the dust shape well enough to allow us to reliably isolate the refractory soot distribution. At higher dust concentrations this approach can lead to an underestimate of residual soot.

The strong relationship in Fig. 6b also confirms the linear relation between $V_{ref<75 -Dust}$ and the absorbing component. BC does not break down in air until heated above 700°C [*Smith and O'Dowd*, 1996]. Hence, the refractory $V_{ref<75 -Dust}$ must include the refractory light-absorbing BC that dominates the light absorption coefficient. Other likely components of the refractory aerosol other than dust include non-absorbing (or relatively low absorbing) refractory organic carbon (OC) remaining at over 300°C and fly ash. Related studies in the Indian Ocean Experiment (INDOEX) suggest about half of the refractory mass in this mode can be refractory OC stable at this temperature [*Mayol-Bracero et al.*, 2002] as discussed in section 3.9.

Following the approach described for Figure 6 we again show our sub-μ extracted refractory soot volume, $V_{ref<75 -Dust}$ (measured every 90 s), only now plotted against the measured PSAP **total** absorption coefficient for both TRACE-P and ACE-Asia experiments (Figure 7). There are fewer data points for TRACE-P because measurements of absorption were cycled between total and sub-μ (aerodynamic) while two PSAP instruments provided continuous data for ACE-Asia. This cycling for TRACE-P also introduces some intrinsic scatter in TRACE-P absorption data because measurements are sequential and not coincident in time. Even so, $V_{ref<75-Dust}$ is closely related to total absorption in TRACE-P with an $R^2$ of 0.94.

The ACE-Asia data in Figure 7 also shows this strong relationship with a slope similar to TRACE-P but there are some groups of data that lie above this slope and also below this slope. We note that the few high values for $V_{ref<75 -Dust}$ evident in Figure 7 that fall above the primary linear relationship are not associated with elevated dust. These anomalous cases are generally from the Yellow Sea and we believe they reflect high concentrations of spherical sub-μ particles characteristic of low-absorbing coal fly-ash. These were often found in large quantities during industrial coal feeding operations near Beijing during 2001 [*Shi et al.*, 2003] and most had diameters below 0.3 μm. This is also consistent with small glasslike cenospheres of $SiO_2$ generated by low-temperature coal combustion from old power plants that have been identified in this region (T. Cahill, personal communication 2002; J. Anderson, personal communication,

2002). Cases below the regression line reveal a higher absorption than can be accounted for by $V_{ref<75\ -Dust}$. This additional absorption is not related to BC but to dust, as evident for cases highlighted when coarse dust volumes exceeded about 200 $\mu m^3 cm^{-3}$ (or about 500 $\mu g\ m^{-3}$ - a moderate but arbitrary choice). Note that the TRACE-P data where very little dust was encountered has very few cases below the regression line. This plot is a useful way to identify most refractory dust, soot, flyash through their "signatures" in their refractory sizes and optical effects.

### 3.6 Refractory Size Distributions and Absorption: The Dust Refractive Index

We determine the best refractive index for the Asian dust by establishing consistency between measured and calculated scattering, absorption and $\varpi$ for both the total and sub-$\mu$ OPC size ranges. Because we must extract the dust size distribution from the total to get the soot components, we focus first on dust by analyzing observations during the heaviest dust case encountered during ACE-Asia Flight 13 in the Yellow Sea. This allows us to examine the limiting behavior for dust absorption. The volatility data (Figure 2) reveals a low soot component for the leg near 5.5 km but higher soot concentrations near the surface. Consequently, we use these cases to help illustrate, explore and constrain the real and complex refractive indices for the absorbing dust and soot components.

The heated and unheated size distributions during this period (eg. Figure 2) indicate that most particle volume is refractory dust with some volatile particles in the accumulation mode. We assume that dust is the dominant coarse particle absorber for highest dust concentrations in these cases. Therefore, the complex refractive index for the observed dust size distribution that generates the observed absorption should be the maximum value for the dust. The presence of additional stronger absorbers (eg. BC) would mean that the contributions from dust to measured coarse PSAP absorption could be even less. Our approach assumes that the influence of a small amount of absorption on OPC derived scattering is negligible. For the absorption considered here this was calculated to be less than 5%. The imaginary part of the refractive index of dust at 550 nm wavelength is initially assumed lie between 0.0003 and 0.0052, while the real part was fixed at 1.53 [*Woodward*, 2001]. A percent or so variation about the real part is common in the literature but this yields negligible changes in calculated scattering. Hence, the OPC OES diameters of the dust as measured are used directly for the Mie calculations. As mentioned earlier, the actual size of volume equivalent spheres are likely to be smaller than OES since irregularly shaped particles scatter more than equivalent spheres [*Kalashnikova and Sokolik*, 2002; *Koepke and Hess*, 1988; *Mishchenko et al.*, 1997]. However, at this point we are interested in measured and modeled optical properties so it is only the measured OES that concerns us.

Confirmation that scattering calculated from OES sizes is reasonably consistent with the measured nephelometer scattering is based upon comparison of both values calculated over nephelometer measurement angles between 7°-170° (Figure 8) and with Flight 13 data highlighted as in Figure 5. This approach avoids the ambiguity in any error in the truncation correction for the nephelometer when particles sizes are very large [*Anderson et al.*, 1996]. The scattering angle of the OPC is only 35° to 145° and, hence, our OES sizes also assume similar scattering between OES calibration spheres and ambient aerosol outside that angular range. Calculations suggest that this influence is expected to be small but, because side scatter is

relatively enhanced for irregularly shaped particles, we expect a tendency to oversize them by the OPC. Calculated and observed scattering is virtually identical for values below 150 $Mm^{-1}$ where dust influence is small. As scattering increases due to dust the calculated values trend about 10% higher than measured. This may be due to the effect just mentioned and/or a coarse aerosol calibration uncertainty for the OPC coarse sizes or transmission differences to the respective instruments for coarse aerosol.

Our objective is to get a complex refractive index for our dust sizes that is consistent with data measured by the PSAP. However, in comparing PSAP data with OPC sizes we need to be aware of transmission losses for larger particles in the PSAP. We have measured this as a function of OPC effective optical size as a function of flow rate (not shown). We found the PSAP at 1 lpm had a transmission of 50% at 12.5 μm OES and 80% at 7 μm OES. This leads to a small correction for absorption on ACE-Asia at highest dust loadings. The 4 lpm volumetric flow rate on TRACE-P requires larger size dependent corrections but the TRACE-P experiment encountered little dust so, with isolated exceptions, these corrections were negligible.

Application of these results allows us to examine the coarse particle PSAP absorption in terms of the size distribution. To facilitate this we define the volume absorption efficiency, VAE, as the coarse particle absorption seen by the PSAP per unit OES volume seen by the PSAP. We argue that as coarse particle volume increases (high dust) the absorption will be dominated by dust absorption. Hence, when VAE is plotted against coarse particle volume it should asymptote to a value characteristic of the dust. It is this behavior that places strong constraints upon the maximum dust complex refractive index. A plot of this measured VAE vs. coarse dust volume is shown in Figure 9a (the color codes from Figure 5 are preserved here). At lower dust OES volumes the VAE is noisy and variable due to the coarse particle absorption being obtained from a small difference between total and sub-μ absorption. However, as coarse dust absorption increases the noise is reduced and the data are seen to asymptote to values near 0.022 $Mm^{-1}\mu m^{-3}cm^{-3}$. Based upon an assumed density for dust of 2.5 g $cm^{-3}$ and a possible OES volume reduction by 25% due to shape effects (see section 3.7) then this value for OES VAE corresponds to a dust MAE of about 0.07 ±0.02 $m^2g^{-1}$. Mie calculations for the measured OES sizes and these asymptotic VAE values also constrain **k** to fall between about 0.0005 and 0.0007, as indicated.

In Figure 9b we show the calculated values for VAE vs. coarse dust volume for **k** = 0.0006 and how it asymptotes to the expected value. The higher VAE values for dust concentrations below 200 $\mu m^3$ $cm^{-3}$ are primarily a consequence of the sigmoidal size-cut or the PSAP impactor (0.75μm OES) that allows some soot aerosol to be included in the coarse mode. This contribution has less effect as dust absorption increases. Moreover, for these particle sizes the difference between spherical and non-spherical absorption cross sections are calculated to be only about 2% [*Mishchenko et al.*, 1997] and imply that this refractive index applies equally well to the irregular dust aerosol.

### 3.8 The influence of BC upon dust optical properties

Figure 9c shows a plot of sub-μ PSAP absorption vs. coarse PSAP absorption (total less the sub-μ PSAP absorption). We first note that the cloud of all ACE-Asia data in light gray suggests a positive background slope. Due to the short 90s sample time there is considerable scatter present. We have stratified this data for low dust cases only (below 20 μg $m^{-3}$ or 50 μg

$m^{-3}$) and found (not shown) that the slope for this subset of data shows coarse absorption to increase with sub-μ absorption. This indicated that typically 10% of sub-μ absorption shows up in the coarse mode. This Figure also includes the coarse absorption due to dust clearly evident in the highlighted data from Flight 13. This Figure and these observations imply that absorbing soot does exist in the coarse mode in the pollution aerosol independent of the presence of dust. The sigmoidal size cut for the impactor [*Wang and John*, 1988] leads to some BC/soot aerosol being removed by the impactor and not measured by the PSAP in the sub-μ mode. However, large soot aerosol has also been identified in some sources near Beijing [*Shi et al.*, 2003] and can be in larger sizes than we typically retrieve in our extracted soot distributions.

Figure 9d is the same as 9c only the modeled dust absorption using **k** = 0.0006 has been subtracted from PSAP coarse absorption. This clearly reduces absorption for most of the highlighted dust cases to within the cloud of variation for most of the data even for this fast 90s average sampling rate. The cloud of gray circles has also narrowed. This change between Figure 9c and 9d reveals the degree to which coarse absorption was due to dust. Also note that the cluster of data (gray circles) in Figure 9c for sub-μ absorption between 20-30 $Mm^{-1}$ have been separated into values that now have coarse absorption near zero and other value that show little change. The former are cases where coarse absorption was accounted for by dust while the latter imply that considerable coarse soot remains in the coarse mode. We note that individual soot carbon particle aggregates in the Beijing region with SEM diameters larger than 0.7 have been shown to comprise from a few percent to as much as 30% of the total [*Shi et al.*, 2003].

However, Figure 9d shows a significant number of data points still to the right of the cloud of data even after correcting for dust absorption. We have examined these cases individually and they are not the highest dust cases. This could indicate another dust type with a higher **k** value but since highlighted green and red data are for two legs through the same plume this seems unlikely. Many of these cases did occur in low-level pollution when some of the lowest ϖ values near 0.7 were observed. Even so, when we stratified for low dust cases there were very few examples of coarse absorption due to coarse soot exceeding about 8 $Mm^{-1}$. Hence, we do not believe these data arise from an underestimate in dust absorption due to larger dust not characterized by the OPC. Rather we believe that they are due to larger absorbing aerosol either with or attached to the dust as seen by the PSAP (eg. see Fig. 2).

### 3.9 Refractory Size Distributions and Absorption: Soot

We have shown that the accumulation mode is predominately internally mixed with a refractory soot component often dominated by absorbing BC. Refining the characteristic shape of the optically effective dust component allowed us to remove its contribution to sub-μ aerosol refractory volume and to better determine the refractory soot-only volume. These considerations and the strong relationship between volatility and soluble ions [*Howell et al.*, submitted 2004] allow us to make assessments of how size-resolved scattering and absorption provide constraints on aerosol intensive properties such as effective real and complex refractive indices and the size resolved mass scattering efficiency (MSE) and mass absorption efficiency (MAE).

Mie calculations of the size-dependent optical properties of soot and dust aerosol are based upon our measured OES diameters shown in Figure 10a. Here we employ the OES dust refractive index 1.53 –0.0006i as determined above and a BC refractive index of 1.95 – 0.66i representative of BC in diesel soot [*Bergstrom*, 1972; *Fuller et al.*, 1999]. The complex refractive index of soot mixtures (BC + refractory OC + volatiles etc.) will also be lower

depending upon the fraction of absorbing BC they contain. Figure 10b shows that the calculated MAE for "pure" BC diameters near 0.2 μm approaches a peak near 6 $m^2g^{-1}$ and a constant value near 4 $m^2g^{-1}$ for much smaller sizes. Calculated MAE values continually drop with an inverse dependence on size above about 0.3 μm due to incident light being absorbed in the surface layer of the BC particles while the shielded mass toward the center does not contribute to absorption. Thus the large EC hollow "balls" shown in Figure 4 contribute a lot to EC absorption measurements but have low BC mass. If we assume that BC has the same size distribution as the sub-μ refractory aerosol sizes (Fig. 10a) then the integral effective MAE is calculated at about 4.7 $m^2g^{-1}$. However, BC aerosol are often made up of smaller BC primary sizes near 0.1 μm such that the MAE of the cluster can be close to the MAE of the primary particle (FMK). As a result, BC integral MAE for pure BC with this refractive index may lie between 4.7 and 6 $m^2g^{-1}$.

These and other more complex effects (see FMK.) need to be considered. However, if we simply apply the refractive indices already mentioned to the size distributions shown in Fig. 10a for soot and dust we obtain the size distributed absorption for the soot and dust components shown in Figure10c. The magnitude of the absorption from BC and dust vary with their relative contributions to the aerosol but the peak in the BC absorption contribution is near diameters of 0.3 μm while that of dust is at diameters over an order of magnitude larger. Figure 10d illustrates the calculated size dependent values of ϖ for the typical dust, pure BC and mixtures of soot and soluble species. We used a volume weighted mixture of BC and volatiles etc. (82% volatile, 6.33% BC and 12.66% refactory OC, see below) in the sub-μ accumulation mode as suggested by our volatility and refractory OC fractions observed in INDOEX [*Mayol-Bracero et al.*, 2002]. This model of homogenous mixing is not realistic (FMK) but provides a sense of possible optical properties. The sub-μ values of ϖ for the dust component are essentially 1 but drop to about 0.9 for OES diameters near 10 μm. Values of ϖ calculated for the mixed aerosol sizes between 0.15 and 0.75 μm are seen to range from about 0.7 to 0.86 depending upon variations in the effective volume (mass) mean diameters for this mode (commonly between 0.2 and 0.5μm). These are much higher than indicated values for pure BC that are near 0.44 at diameters near 0.2 μm. Actual values will probably differ due to various aspects of the mixing state not considered here (see FMK).

## 4.0 Refractory Soot, BC and EC relationships and MAE values

The mass absorption efficiency, MAE, for the BC aerosol can be obtained from measured PSAP absorption and the estimated mass of absorbing carbon. Measurements of elemental carbon mass, EC, based upon $CO_2$ evolved from heated samples can also be related to aerosol light absorption and the refractory size distribution containing BC. A variety of EC techniques are used which differ in their approach and the manner in which EC is operationally defined, [*Lim et al.*, 2003]. ACE-Asia employed the approach developed by Sunset Labs [*Huebert et al.*, 2003]. Leg average values for EC of about 30 min duration were required in order to obtain a reasonable signal to noise ratio. These leg average regressions between BC absorption, refractory volume and EC are shown for the ACE-Asia data in Figure 11a for data below 2km where higher concentrations generally give EC data its best signal to noise. Four very anomalous values for EC were removed because they were not expressed in either BC absorption or OPC refractory volumes.

Figure 11a shows that EC is related to both sub-μ and total measured PSAP absorption with an $R^2$ of about 0.40. Uncertainty arises both through some measurements being near detection limits and as a result of the operational definition of EC that includes the correction for charring of OC to BC [*Huebert et al.*, 2003]. The two indicated regression slopes for total and sub-μ absorption yield an MAE of 6.1 and 8.1 $m^2g^{-1}$. As we mentioned in the discussion of Figure 9, on average about 10% of the total soot absorption was commonly in the PSAP coarse size range. Hence the EC measurement on the total aerosol is best compared to the total PSAP absorption for most samples. However, the larger MAE values for the PSAP total data also include additional absorption due to dust. Solid circles highlight data for high dust with coarse volumes greater than 200 $\mu m^3cm^{-3}$ and reveal the role of dust in generating outliers for this relationship. With these considerations in mind, the MAE for BC based upon the limited EC measurements and their uncertainty indicate a representative value of about $7 \pm 2$ $m^2g^{-1}$.

As demonstrated in Figures 7 and 8, the absorbing BC is a dominant part of the sub-μ refractory volume with dust removed. The plot of $V_{ref<75\text{-}Dust,}$ against EC in Figure 11b has an $R^2$ value of about 0.46. If we assume that $V_{ref<75\text{-}Dust}$ is pure BC with an estimated density of about 1.9 g $cm^{-3}$ (FMK) then the estimated mass of this $V_{ref<75\text{-}Dust}$ exceeds corresponding EC values by a factor of about 2.2. If we assume the EC is the absorbing BC then this would suggest 45% or so of our $V_{ref<75\text{-}Dust}$ is absorbing BC on average. This is in line with thermo-optic analysis for other Asian aerosol (INDOEX; [*Mayol-Bracero et al.*, 2002]) that found the $CO_2$ evolved at temperatures above 300°C includes refractory OC that contributes about 60±10% of the CO2 evolved from BC mass. Little other refractory mass was reported by these authors.

Figure 11c shows $V_{ref<75\text{-}Dust}$ data averaged over flight legs corresponding to the EC measurements. It demonstrates that $V_{ref<75\text{-}Dust}$ is far better correlated with sub-μ BC absorption ($R^2$ about 0.79) than with EC ($R^2$ about 0.40). This shows that EC measurement uncertainty is a source of the lower correlations in Figure 11a and 11b and encourages our use of refractory volume to assess MAE for the soot/BC combinations. In order to estimate the MAE of the absorbing BC based upon our OPC $V_{ref<75\text{-}Dust}$ data we need to account for proper conversion of OES volumes to refractory aerosol mass and the absorbing BC component. Adjustments for the OPC sizing should be applied for highly absorbing aerosol [*Pinnik et al.*, 2000] and we have previously noted oversizing of about 8% by the OPC for pure BC aerosol with diameters below about 0.4 μm [*Clarke*, 1991]. However, because our $V_{ref<75\text{-}Dust}$ is expected to be less than half BC by volume, we expect a smaller effect of say 3% such that actual sub-μ refractory volumes are estimated to be about 90% of measured OPC OES volume. However, the sigmoid cut of the PSAP impactor also removes about 10% of the BC as estimated from our OPC $V_{ref<75\text{-}Dust}$ (Fig. 9 discussions). Consequently, these effects should be compensating when we compare $V_{ref<75\text{-}Dust}$ with mean sub-μ PSAP values, as in Figure 11c.

Furthermore, the actual OC mass during ACE-Asia is related to the measured $CO_2$ evolved from OC by a multiplier of about 1.4 [*Russell*, 2003] based upon separate analysis of OC functional groups for ACE-Asia. We assume here that the refractory OC in ACE-Asia and TRACE-P experiments has the same proportion of $CO_2$ evolved relative to BC (ie. 60±10%) as in INDOEX. However, the multiplier used on INDOEX was assumed to be 1.7 when correcting to OC mass [*Mayol-Bracero et al.*, 2002]. Application of the 1.4 multiplier to the $CO_2$ evolved from the refractory OC implies that the actual refractory OC mass is about 85% of the BC mass. Hence, for an OC density of 1 g $cm^{-3}$ and BC near 1.9 g $cm^{-3}$ (FMK) we expect 40% of our volume, $V_{ref<75\text{-}Dust}$, will be BC and 60% will be OC. Hence, if 40% of $V_{ref<75\text{-}Dust}$ is BC with a density of 1.9 g $cm^{-3}$ then we can convert the indicated slope in Figure 11c to an MAE for BC by

dividing by 0.4 and dividing by density. This yields an MAE = 6.7 $m^2g^{-1}$. We recognize the OC volume fraction is poorly constrained. However, the high correlation in Fig. 7 implies that this fraction does not vary widely between ACE-Asia and TRACE-P and we expect the latter BC sources to be similar to INDOEX values. Consequently, if we consider the refractory OC fraction (as $CO_2$) for INDOEX to range from 50% to 70% then we get an uncertainty in our MAE of 6.7 ± 0.7 $m^2g^{-1}$. Alternately, if this assessment were made assuming the 1.7 multiplier mentioned above for conversion to OC mass instead of 1.4 then the MAE would be 7.6 ± 0.8 $m^2g^{-1}$. These values are also remarkably consistent with the range of values based upon EC estimated from Figure11a.

It is important to keep in mind that these MAE values are for the BC mass are obtained from the measured PSAP absorption for the internally mixed sub-μ aerosol. This includes possible enhancements to pure BC absorption arising from the state of mixing (FMK). Higher MAE values for BC would also be obtained if BC were a smaller fraction of the refractory component (ie. BC+ high temp OC) than used above. However, a smaller fraction would be inconsistent with most INDOEX data (Mayol-Bracero, personal correspondence 2003) and the relation indicated in Figure 11b. This implies that the range of MAE values above should be representative of these data sets.

### 4.1 The influence of dust on BC optical properties

Earlier we indicated a possible perturbation of dust optical properties arising from the coagulation of BC with the dust mode. However, the presence of dust surface area can also be expected to influence the accumulation of volatiles including sulfuric acid and OC vapors [*Tang and al.*, 2003]. In the absence of enhanced Asian dust these species commonly reside in the accumulation mode and on other coarse pollution aerosol (eg. Figure 3 bottom). Because these species are associated with the combustion source regions we might expect them to be found in characteristic ratios with BC for a given region and time. Also, because the BC component is formed at high temperatures in the combustion process, these volatile components will be added to the BC after its emission. Condensates like combustion derived OC may promptly deposit to aerosol surface while others, like sulfates, would take longer because photochemical processes are required. If BC is generated and emitted into dusty air with elevated surface area, then significant fractions of these components may accumulate on the dust instead of becoming associated with soot/BC in the accumulation mode.

Figure 12a shows the ratio of the refractory volume, $\mathbf{V_{ref<75\text{-}Dust}}$, to total accumulation mode aerosol, $\mathbf{V_{tot<75\text{-}Dust}}$ (dust removed), obtained from our OPC volatility data. This data is from all ACE-Asia horizontal legs below 2km altitude and shown for over three decades of coarse particle volume along with average values binned over equal log intervals of coarse particle volume. These average values are presumed to reflect regional characteristics for the ACE-Asia domain during April 2001. Coarse particle volume includes contributions from typical background dust, industrial dusts or fugitive emissions as well as significant Asian Dust transport events moving through the region. These coarse volume values can be put in context when compared to $PM_{10}$ data for urban Beijing in 2001. A weekly average in March was about 360 μg $m^{-3}$ (150 $\mu m^3cm^{-3}$) and in April was 200 μg $m^{-3}$ (80 $\mu m^3cm^{-3}$) while in the low-dust and low heating-fuel period of September it was about 130 μg $m^{-3}$ (50 $\mu m^3cm^{-3}$) [*Shi et al.*, 2003]. In view of these values we assume that our Fig. 12 data collected in April 2001 will represent

strong urban pollution signatures for coarse volumes in near 50-80 $\mu m^3 cm^{-3}$. We assume that values much larger than this indicate enhanced incursions of Asian dust into the region.

There is a very gradual decrease in the sub-μ refractory volume ratio when coarse volume is below about 50 $\mu m^3 cm^{-3}$. However, when coarse volumes exceed this value the sub-μ refractory volume fraction of the accumulation mode [$\mathbf{V_{ref<75\text{-}Dust}}$ /$\mathbf{V_{tot<75\text{-}Dust}}$] clearly increases as the dust volume increases. Because $\mathbf{V_{ref<75\text{-}Dust}}$ is emitted from combustion sources it should vary due to the presence of dust. Hence, we argue that this ratio changes due to the loss of volatiles from this mode to the coarse dust surface. This leads to an increase in the soot/BC fraction left in the accumulation mode.

This is confirmed in Figure 12b where we plot volatile volume below 0.75 μm as measured by the OPC vs. the coarse mode volume. The volatile volume below about 1.2 μm as expected to be measured by the PILS and the actual PILS combined mass for sulfate, nitrate and ammonium ions are also indicated and display a similar behavior. Peak values are evident for coarse concentrations near 80 $\mu m^3 cm^{-3}$, as would be expected for values representative of the polluted urban environment. As dust concentrations increase to over 500 $\mu m^3 cm^{-3}$ ( 1,500 $\mu g^3 m^{-3}$) these volatile species and soluble ions drop to about half of their peak values consistent with the increase of $\mathbf{V_{ref<75\text{-}Dust}}$. Also note the consistency in the drop of for both measured PILS mass and the volume estimated for the PILS from the OPC data. The more rapid drop seen in the [$\mathbf{V_{ref<75\text{-}Dust}}$ /$\mathbf{V_{tot<75\text{-}Dust}}$] dust is also expected since it reflects only those sizes below 0.75 μm whereas the other plots include the material on the tail of the dust distributions.

When coarse volumes drop well below 50 $\mu m^3 cm^{-3}$ the volatile volume and the PILS ionic mass (Fig. 12b) also decrease dramatically while the [$\mathbf{V_{ref<75\text{-}Dust}}$ /$\mathbf{V_{tot<75\text{-}Dust}}$] (Fig. 12a) changes slowly. This can be understood in view of the range of locations and altitudes represented in this data set. Scattering and absorption (and associated refractory sub-μ aerosol) decrease with altitude and the variability is large (Fig. 1). Below 2km this variability is often due to dilution of near surface air by mixing with clean air aloft. Clean air can often have very low concentrations of both refractory and volatile aerosol. Hence, mixing will generally dilute near surface pollution concentrations but preserve the ratio [$\mathbf{V_{ref<75\text{-}Dust}}$ /$\mathbf{V_{tot<75\text{-}Dust}}$]. Clear air aloft also tends to have a greater fraction of more volatile non-absorbing aerosol [*Clarke et al.*, 1997] that is consistent with the gradual decrease in refractory volume and increase in ϖ (Fig. 12a) as coarse volume decreases.

We demonstrated earlier (Figures 2) that BC in the accumulation mode usually contributes only a small fraction of the total accumulation mode volume even though it dominates the absorption. Hence, the scattering properties of the accumulation mode are generally dominated by the volatile/soluble component often accumulated on the soot aerosol. Consequently, when the refractory fraction of the accumulation mode increases we might expect the value of sub-μ ϖ to decrease. This is shown to be the case in Figure 12 where the lowest values of sub-μ ϖ are associated with the highest dust cases and trend down with an increasing refractory volume fraction present in the accumulation mode. Although the dust tail present in the sub-μ mode contributes refractory aerosol with ϖ near 1 (see Figure 10b), the reduction in scattering due to loss of volatile species has the greater effect. The result is lower measured sub-μ ϖ values in the high-dust cases even though ϖ for the total aerosol increases due to dust. The strong relationship between these two trends is evident when we plot the co-albedo (1-ϖ) against the refractory volume fraction from the binned average data in this figure, as shown in the inserted panel. This relation has a slope of 0.68 and an $R^2$ of 0.94 indicating a strong average regional influence of

dust upon the optical properties of the pollution mode aerosol. We will return to this and related issues in the discussion.

## 4.0 Comparison of measured BC to model values

One of the objectives of TRACE-P and ACE-Asia was to obtain information on aerosol and gas phase properties over scales and times that could be used to challenge chemical transport models (CTM). Several modeling groups were involved with these experiments but the University of Iowa group [*Carmichael et al.*, 2003] employed their CTM in support of both experiments and included the modeling of BC. In Figure 13 we present some initial comparisons of measured and model results for both $BC_{model}$, measured PSAP light absorption and $V_{ref<75-Dust}$ for both campaigns. Because each point is a measurment of only 90s it captures details of atmospheric variability not resolved on the scales of the model or the meteorological data that the CTM is based upon. Hence, a strong pointwise comparison is not our objective but rather we are interested in broad indications of consistency or inconsistency with regional model data.

Figure 13a shows PSAP absorption vs. $BC_{model}$ for TRACE-P where biomass plumes were common and dust absorption was negligible. It is stratified here by the ratio of $CO_{measured}$ to $CO_{model}$ for values above and below a value of 1.2. This provides a gauge of model performance for combustion derived CO where ratios larger than 1.2 indicate model underestimates for CO. The slopes shown on Fig. 13a are the $MAE_{model}$ for the model when evaluated based upon measured PSAP absorption and $BC_{model}$. The regression for cases when the $CO_{model}$ is within 20% of measured values has a slope of 7.7 $m^2g^{-1}$ while for the cases when $CO_{model}$ underestimates observed values the regression is about 17 $m^2g^{-1}$. The former is consistent with expected MAE values determined above while the latter value is high and indicative of the $BC_{model}$ being too low.

Figure 13b shows a similar plot for ACE-Asia. However, biomass sources were a much smaller contributor to BC emissions in this region [*Ma et al.*, 2003; *Uno et al.*, 2003]. Here the data clearly suggest two branches. We have selected two constraints for the data to emphasize conditions where CO sources in the CTM inventory CFORS , [*Streets et al.*, 2003; *Uno et al.*, 2003] were dominated by model combustion fuel sources (CFORS fuel CO >20ppbv) and when they were dominated by biomass (CFORS biomass CO > 10 ppbv). These two dominant source types fall into the two separate branches. The biomass sources dominate the lower branch with a $MAE_{model}$ of 7.2 $m^2g^{-1}$ based upon an average for the constrained data, very similar to the TRACE-P value in Fig. 13a. The upper branch indicates a typical $MAE_{model}$ value near 32 $m^2g^{-1}$ and clearly about a factor of three or more higher than can be justified.

Figure 13c shows an analysis similar to Figure 13b and demonstrates that our $V_{ref<75-Dust}$ vs. $BC_{model}$ reveals clearly the same features. In Figure 13d we again return to our signature plot of $V_{ref<75-Dust}$ vs. PSAP absorption (Fig. 7) only for the ACE-Asia data shown with the same two constrained and highlighted data sets. This plot confirms that highlighted CFORS biomass and CFORS fuel dominated cases fall along the same slope. This slope is the VAE (proportional to MAE) for absorbing BC and implies differences of less than 10% in MAE for the two fuel types. This demonstrates that both soot aerosol sources in the model have similar observed optical properties so that soot microphysics or optics cannot be a reason for these differences. Hence, these observations indicate that current estimate of emissions by *Streets et al.*[*Streets et al.*, 2003] used in CFORS for biomass BC appear to be consistent with our MAE for TRACE-P and

ACE-Asia but that combustion fuel BC in the region north of 25°N may be a factor of 3 or so too low.

## 5. Discussion and Conclusion

Thermal analysis of the size distributions of Asian aerosol provided insight into its physio-chemical properties. This approach demonstrated that BC and associated high temperature emissions establish most of the aerosol number concentration by providing sites upon which other species (eg. sulfate, nitrate, water) condense and/or heterogeneously react. These soluble species and organic components were mixed with soot in over two thirds of the aerosol and constituted most of the sub-μ volatile volume. TDMA data indicates that within the accumulation mode the refractory soot fraction is generally 10 to 25% of the total volume for sizes near 0.1 μm.

Optically effective dust sizes were measured out to 14μm. Examination of coarse particle absorption per unit volume of dust as dust volume increases resulted in asymptotic values that constrain the complex refractive index for dust. These values were consistent with the measured absorption and scattering coefficients and imply a refractive index for Asina dust of n = 1.53 - 0.0006i (±0.0001i) when used for optically effective sizes. Unlike BC, the MAE for dust OES has a maximum of about 0.07 $m^2 g^{-1}$ near 2 μm. These optical properties results in ϖ values for the dust distribution that vary from about 1 for sub-μ sizes up to about 0.93 at 10μm diameter, consistent with the effective coarse particle ϖ values observed near 0.97 (Anderson et al., 2003) for dust dominated cases. Optical properties were often well described by the presence of an accumulation mode with ϖ near 0.84 and a dust aerosol with ϖ near 0.97. Variations in relative contributions from both types account for significant variation in total ϖ observed. The statistically larger values for ϖ seen for Asian aerosol south of 25°N (TRACE-P) and those seen during ACE-Asia are explained by the greater prevalence of dust mixed with aerosol north of 25°N.

In cases of pollution in the presence of high dust concentrations, we observed larger refractory soot fractions in the accumulation mode and correspondingly lower sub-μ ϖ values than for the case of pollution with low dust. Dust should increase sub-μ ϖ because ϖ is near 1 for sub-μ dust (Figure 10d). Hence, this decrease must be due to the relative increase in the BC fraction of the accumulation mode as a result of uptake of volatile species onto the dust. This average influence can be quantified by making an approximate straight line fit in Figure 12 between the soot volume ratio at about 80 $\mu m^3 cm^{-3}$ and about 500 $\mu m^3 cm^{-3}$ to get a linear expression for this ratio as a function of the logarithm of coarse mode volume, $\boldsymbol{D}_{v,}$. When combined with the linear expression between this ratio and co-albedo from the insert plot one gets the following expression for ϖ in terms of $\boldsymbol{D}_v$.

$$\boldsymbol{\varpi} = 0.84 - 0.102 \log (\boldsymbol{D}_v/80) \qquad \text{where } \boldsymbol{D}_v \text{ is OES dust volume in } \mu m^3 cm^{-3} \qquad \text{(Eqn. 1.)}$$

In order to express this in terms of a more familiar mass concentration we not only have to use a dust density of about 2.5 g $cm^{-3}$ to convert volume to mass but also must correct OES to geometric diameter. The latter is not well constrained but for the angular range of our OPC of 35° to 145° the greatest change in scattering intensity for irregular dust relative to spheres occurs

around 100° to 145° [*Kalashnikova and Sokolik*, 2002] but this is also where the phase function also has minimum values. We estimate from their assessment that the change in integral OPC scattering intensity due to shape effects is less than 20%. This will increase our OES diameter by less than 10% and our optical volume by less than 25% over an equivalent mass dust. This is probably an upper limit of the shape effect on our OPC measurements and smaller effects are likely (Kalashnikova, personal correspondence, 2003). Hence, the expression above can by employed as an approximation when applied to measured dust mass, $\boldsymbol{D_m}$ by replacing the term $\boldsymbol{D_v}$/80 by $\boldsymbol{D_m}$/160 [ie. 160=80x2.5/1.25] where $\boldsymbol{D_m}$ is in μg $m^{-3}$. As an example, our regional pollution aerosol has a typical sub-μ ϖ of about 0.84 in the absence of high dust (Figure 12). When it is emitted into a mean dust concentration of 1000 μg $m^{-3}$ (about 500 $\mu m^3 cm^{-3}$ OES) then Eqn. 1 predicts the value of sub-μ ϖ to be reduced to 0.76 due to transfer of volatiles to the dust.

This change in sub-μ ϖ is a result of the transfer of volatile mass from the accumulation mode to the dust. A detailed optical model of this effect must take into account the complex interaction of BC with condensed species (see FMK) at a level beyond the scope of this paper. However, some insight can be gained through a simple examination of the dependency of ϖ on $MAE_a$ and $MSE_a$ for the accumulation mode mass, $m_a$. We can write this as follows:

$$\varpi = \sigma_{sp}\,[\sigma_{sp} + \sigma_{ap}]^{-1} = [1 + \sigma_{ap}/\sigma_{sp}]^{-1} = [1 + (\sigma_{ap}/m_a)(m_a/\sigma_{sp})]^{-1} \qquad \text{(Eqn. 2 )}$$

$$\varpi = [1 + MAE_a / MSE_a]^{-1}$$

where $\sigma_{sp}$ and $\sigma_{ap}$ are the particle scattering and absorption coefficients respectively.

We assume here an internal mixture of soot/BC with volatiles and the absorption is not significantly affected by this loss of volatiles. Hence, the $MAE_a$ for the accumulation mode mixture will change primarily in response to the loss of volatile mass from the accumulation mode to the dust. Our data in Figure 12 indicates that about half the volatile volume (about 40% of the total volume) is lost to the dust when concentrations rise from about 80 $\mu m^3 cm^{-3}$ characteristic of urban pollution to 800 $\mu m^3 cm^{-3}$ in high dust events. At the same time the refractory fraction increases from 20 to 30% of the total (Fig. 12a). Ignoring density differences, this loss of 40% volatile volume implies that the $MAE_a$ will increase by about a factor of 1.6. At the same time this loss will reduce the remaining accumulation mode to 0.6 of its original volume or about 85% of its original diameter. This size change will also decrease the effective $MSE_a$ by about 15% or so for this aerosol (see Fig 10b). Consequently, the net effect of this high dust on Eqn. 2 will be to change the ratio of $MAE_a$ to $MSE_a$ by a factor of about 1.6/0.85 = 1.9. Our observed regional average sub-μ ϖ in pollution with a coarse volume of 80 $\mu m^3 cm^{-3}$ is 0.84 (Fig 12a). Eqn. 2 indicates that this corresponds to a ratio of $MAE_a$ to $MSE_a$ of 0.19. When this value is multiplied by the factor 1.9 then the new value for ϖ under high dust predicted by Eqn. 2 is about 0.73 and in good agreement with Figure 12a for a coarse volume of 800 $\mu m^3 cm^{-3}$. Hence, this simple approach demonstrates that the transfer of volatile material to the coarse dust mode is quantitatively linked to a corresponding change in sub-μ ϖ. We plan a more detailed investigation of this effect in a later paper.

The amount of volatiles that can be expected to accumulate on the dust will depend upon the dust surface area, how long it is available for these species to interact with the dust, the dust surface chemistry, the chemistry of the accumulating species, the concentrations of the

accumulating species and environmental process and conditions etc. Even so, our data (Figure 12a, b) reveals that about 50% of the volatiles normally in the accumulation mode when no dust is present get transferred to the dust when high dust concentrations mix with pollution in this region. Model calculations by *Tang et al* [*Tang and al.*, 2003]for similar dust concentrations indicate that about 30% of the sulfate and 80% of the nitrate can end up on the dust surface. Keeping in mind that our volatile components can include these species as well as some volatile OC we believe that our observations are consistent with their model and tend to confirm the magnitude of their model results.

This effect will result in accumulation of this scattering mass onto larger dust sizes with low effective MSE instead of onto the optically effective accumulation mode. As a result, the contribution to scattering extinction by these emissions (eg. sulfate) will decrease about an order of magnitude for mass transferred from sizes at 0.3 μm to sizes at 3.0 μm (see Fig. 10b). Hence, column optical depths or radiative forcing estimated from regional sulfur emissions can be in error as a result their uptake onto the dust. Sub-μ ϖ will also be lowered compared to what might be expected if the pollution and dust modes were separately modeled with no interaction. Consequently, the optical properties of a mixture of dust and pollution aerosol will be different if they mix before or after most volatiles have been adsorbed. This means that the physical, chemical and optical properties of pollution and dust aerosol that mix near sources are not additive for each source but must be modeled interactively. It also means that regional emissions of species such as sulfate cannot simply be scaled to a net radiative forcing without considering the aerosol environment they are emitted into.

Comparison of PSAP light absorption with EC measurements indicated measured MAE values for EC lie in the range of about $7 \pm 2$ $m^2g^{-1}$ (Fig. 11a). However, the correlation coefficient with EC was $R^2$=0.4 so considerable scatter in the data is present. Thermally resolved OES sub-μ refractory volume was more highly correlated with sub-μ PSAP absorption ($R^2 = 0.79$) indicating that this refractory volume distribution contains the absorbing BC (Fig. 11c). This refractory volume is known to also include OC remaining at 300°C [*Mayol-Bracero et al.*, 2002] where the latter can equal about half of the refractory mass (about 1/3 the refractory volume). MAE values based on this data were shown to lie in the range of 6 to 8.4 $m^2g^{-1}$, consistent with the EC analysis. The comparison of EC and the refractory soot volume was also consistent with the INDOEX estimate of BC being about one half of the refractory sub-μ mass. These MAE values are also similar to data for BC measured on aircraft in INDOEX reported as 6.6 to 8.1 $m^2g^{-1}$ [*Mayol-Bracero et al.*, 2002] and to the MAE values inferred from the model data discussed for TRACE-P and ACE-Asia.

BC in the accumulation mode tended to have OES volume mean diameters near 0.3±0.2μm. Mie calculations using the OPC refractory volume distributions and a refractive index of 1.95 – 0.66i were shown to yield a size-weighted sub-μ MAE of about 4.7 $m^2g^{-1}$ for the pure BC component when treated as BC spheres over the refractory OES size ranges. This is considerably lower than the values obtained above even though our assumed value of **k** = 0.66 is relatively high and mean values higher than this are not easy to justify. We believe that these differences probably arise due to enhancement effects arising from the internal mixture of BC with OC, sulfate and other species. If large BC aerosol are aggregates of primary aerosol with sizes of 0.1–0.2 μm diameter then larger BC clusters would have properties more like the primary sizes. This would yield MAE values closer to the peak value of 5 to 6 $m^2g^{-1}$ in Figure 10b. If the BC were usually on the surface of the accumulation mode aerosol then an additional enhancement of 15% might raise average values to 6 to 7 $m^2g^{-1}$ as per FMK. Additional

enhancements from some BC being encapsulated in OC and volatile aerosol at the 10-20% BC volume fraction level could also increase these values for certain sizes. Such enhancements in absorption due to prescribed mixtures of BC and OC for sizes similar to our soot distributions have been recently demonstrated to approach a factor of 2 in the laboratory [*Saathoff et al.*, 2002]. Even so, if we allow for the probability of some BC with lower refractive indices than assumed here, the evidence for some BC present at larger sizes, a variable range of morphology, a variable state of mixing, etc. then an average values of a factor of two enhancement for Asian BC appears unlikely. Consequently, our MAE values above suggest a moderate enhancement of perhaps 50% over MAE values expected for pure BC but consistent with the most likely values estimated by FMK. These MAE values are lower than values of $11 \pm 5$ $m^2g^{-1}$ reported by [*Mader et al.*, 2002] but within their wide uncertainty range.

A comparison of our BC absorption, refractory volume and CTM model output for the chemical weather forcasting (CFORS) regional emissions indicate that emissions of BC [*Streets et al.*, 2003] encountered during TRACE and during dominant biomass sources during ACE-Asia regions are consistent with our measurements. However, some combustion fuel sources appear underpredicted by the model by about a factor of 3. This is similar to underpredictions of CO also seen in the model for similar sources [*Streets et al.*, 2002; *Tang and al.*, 2003]. Other model results that employ the same emission inventory have found regional differences in measured and model BC that have been attributed to measurement differences [*Uno et al.*, 2003]. However, the model underestimates of BC indicated here can be expected to contribute significantly to these regional differences.

BC is a primary emission upon which many other components condense to create an internal mixture. Hence, BC accounts for about 75% of the observed accumulation mode number. As a result, the nature of the combustion process and how BC emissions and the number of BC particles are generated has implications for both direct and indirect forcing. Moreover, these results demonstrated that details of BC microphysical properties and its optical effects must be considered in conjunction with condensates associated with it as well as the full aerosol size distribution into which they are mixed.

**Acknowledgements:**

This data collection and analysis was only possible through the combined support provided for TRACE-P (NASA NCC-1-416) and ACE-Asia grant support (NSF ATM00-02070). We are particularly grateful for the chief scientists D. Jacob, J. Crawford and B. Huebert and support crews of the NASA p3B and NCAR C-130. Special appreciation is extended to Program Managers, Vickie Connors (NASA) and Anne-Marie Schmoltner (NSF), for encouraging and supporting the inter-comparison flights between the two programs that facilitated combining these data sets.

**References**


Alfaro, S.C., A. Gaudichet, L. Gomes, and M. Maille, Mineral aerosol production by wind erosion: aerosol particle sizes and binding energies, *Geophysical Research Letters*, *25*, 991-994, 1998.

Anderson, T.L., Variability of aerosol optical properties derived from in situ aircraft measurements during ACE-Asia, *Juour. Geophys. Res.*, 2003.

Anderson, T.L., D.S. Covert, S.F. Marshall, M.L. Laucks, R.J. Charlson, A.P. Waggoner, J.A. Ogren, R. Caldow, R. Holm, F. Quant, G. Sem, A. Wiedensohler, N.A. Ahlquist, and T.S. Bates, Performance characteristics of a high-sensitivity three-wavelength, total scatter/backscatter nephelometer, *Journal of Atmospheric and Oceanic Technology*, *13*, 967-986, 1996.

Bergstrom, R.W., Predictions of the spectral absorption and extinction coefficients of an urban air pollution model, *Atmospheric Environment*, *6*, 247-258, 1972.

Bond, T.C., T.L. Anderson, and D. Campbell, Calibration and intercomparison of filter-based measurement of visible light absorption by aerosols, *Aerosol Science and Technology*, *30*, 582-600, 1999.

Carmichael, G.R., Y. Tang, G. Kurata, I. Uno, D. Streets, J.-H. Woo, H. Huang, J. Yienger, B. Lefer, R. Shetter, D. Blake, E. Atlas, A. Fried, E. Apel, F. Eisele, C. Cantrell, M. Avery, J. Barrick, G. Sachse, W. Brune, S. Sandholm, Y. Kondo, H. Singh, R. Talbot, A. Bandy, D. Thorton, A.D. Clarke, and B. Heikes, Regional-Scale Chemical Transport Modeling in Support of the Analysis of Observations obtained during the TRACE-P Experiment, *Journal of Geophysical Research*, 2003.

Clarke, A.D., A thermo-optic technique for *in-situ* analysis of size-resolved aerosol physicochemistry, *Atmospheric Environment*, *25A* (3/4), 635-644, 1991.

Clarke, A.D., and R.J. Charlson, Radiative Properties of the Background Aerosol: Absorption Component of Extinction, *Science*, *229*, 263-265, 1985.

Clarke, A.D., W.G. Collins, P.J. Rasch, V.N. Kapustin, K.G. Moore, S. Howell, and H.E. Fuelberg, Dust and pollution transport on global scales: Aerosol measurements and model predictions, *Journal of Geophysical Research*, *106* (D23), 32555-32569, 2001.

Clarke, A.D., T. Uehara, and J.N. Porter, Atmopspheric nuclei and related aerosol fields over the Atlantic: Clean subsiding air and continental pollution during ASTEX, *Journal of Geophysical Research* (D21), 25821-25292, 1997.

Clarke, A.D., J.L. Varner, F. Eisele, R. Tanner, R.L. Mauldin, and M. Litchy, Particle production in the remote marine atmosphere: Cloud outflow and subsidence during ACE-1, *Journal of Geophysical Research*, *103*, 16397-16409, 1998.

d'Almieda, G.A., On the variability of desert rediative characteristics, *Jour. Geophys. Res.*, *92*, 3017, 1987.

Fuller, K., W.C. Malm, and S.M. Kriedenweiss, Effects of mixing on extinction by carbonaceous particles, *Journal of Geophysical Research*, *104*, 15941-15954, 1999.

Howell, S.G., A.D. Clarke, Y. Shinozuka, V.N. Kapustin, C.S. M$^{c}$Naughton, B.J. Huebert, T. Bertram, J.T. Kline, S. Masonis, T.L. Anderson, R.J. Weber, K. Maxwell-Meier, and D. Orsini, Airborne measurments of aerosol size

distributions and the effect of relatie humidity during ACE-Asia and TRACE-P, *Journal of Geophysical Research*, submitted 2004.

Huebert, B., PELTI: Measuring the Passing Efficiency of an Airborne Low Turbulence Inlet, *Jour. Geophys. Res.*, 2003.

Huebert, B.J., T.S. Bates, P.B. Russell, G. Shi, Y.J. Kim, K. Kawamura, G.R. Carmichael, and T. Nakajima, An overview of ACE-Asia: strategies for quantifying the relationships between Asian aerosols and their climatic impacts, *Journal of Geophysical Research*, 2003.

Jacob, D.J., J.H. Crawford, M.M. Kleb, V.E. Connors, R.J. Bendura, J.L. Raper, G.W. Sasche, J.C. Gille, L. Emmons, and C.L. Heald, The Transport and Chemical Evolution over the Pacific (TRACE-P) Mission: Design, execution and overview of results, *Journal of Geophysical Research*, 2003.

Kalashnikova, O.V., and I.N. Sokolik, Importance of shapes and compositions of wind-blown dust particles for remote sensing at solar wavelengths, *Geophysical Research Letters*, *29* (10), 2002.

Kaufman, Y., D. Tanre, O. Dubovik, A. Karniele, and L. Remer, Absorption of sunlight by dust as inferred by satellite measurements and ground based remote sensing, *Geophysical Research Letters*, *28*, 1479-1482, 2001.

Koepke, P., and M. Hess, Scattering functions of tropospheric aerosols: The effects of non-spherical particles, *Applied Optics*, *27*, 2422-2430, 1988.

Li, J., M. Posfai, P.V. Hobbs, and P.R. Buseck, Individual aerosol particles from biomass burning in Southern Africa:2, Compositions and aging inorganic particles, *Journal of Geophysical Research*, *108* (D13), 8484, doi: 10.1029/2002JD002310, 2003.

Lim, H., B.J. Turpin, E. Edgerton, S.V. Hering, G. Allen, H. Maring, and P. Soloman, Semicontinuous aerosol carbon measurements: Comparison of Atlanta supersite measurements, *Journal of Geophysical Research*, *108* (D7), doi: 10.1029/2001JG001214, 2003.

Ma, Y., D. Orsini, K. Maxwell-Meier, Y.N. Lee, K.G. Moore, V.N. Kapustin, A.D. Clarke, and R.J. Weber, Refinements to the particle-into-liquid sampler (PILS) for ground and airborne measurements of water soluable aerosol chemistry, *Journal of Geophysical Research*, 2003.

Mader, B., R.C. Flagan, and J.H. Seinfeld, Airborne measurements of atmospheric carbonaceous aerosols during ACE-Asia, *Journal of Geophysical Research*, *107*, doi 10.1029/2002JD002221, 2002.

Mayol-Bracero, O.L., R. Gabriel, M.O. Andreae, T.W. Kirschstetter, T. Novakov, and D. Streets, Carbonaceous aerosol over the Indian Coean during INDOEX: Chemical characterizzation, optical properties and probable sources, *Journal of Geophysical Research*, *107* (D19), doi: 10.1029/2000JD000039, 2002.

Mishchenko, M.I., L.D. Travis, R.A. Kahn, and R.L. West, Modeling phase functions for dustlike tropospheric aerosol using shape mixture of randomly orientyed polydisperse spheroids, *Journal of Geophysical Research*, *102*, 16831-16847, 1997.

Moore, K.G., A.D. Clarke, V.N. Kapustin, C.S. McNaughton, B.E. Anderson, E.L. Winstead, R.J. Weber, Y. Ma, Y.N. Lee, R.W. Talbot, J. Dibb, T. Anderson, S. Masonis, D.S. Covert, and D. Rogers, A comparison of similar aerosol

measurements made on the NASA P3-B, DC-8 and NSF C-130 aircraft during TRACE-P and ACE-Asia, *Journal of Geophysical Research*, submitted 2003.

Orsini, D., Y. Ma, A. Sullivan, B. Sierau, K. Baumann, and R.J. Weber, Refinements to the particle-into-liquid sampler (PILS) for ground and airborne measurements of water soluable aerosol composition, *Atmospheric Environment*, 2003.

Pinnik, R.G., J.D. Pendelton, and G. Videen, Response characteristics of particle measurement systems active scattering spectrometer probes, *Aerosol Science and Technology*, *33*, 334-352, 2000.

Russell, L., M., Aerosol Organic-Mass-to-Organic-Carbon Ratio Measurements, *Jour. Geopys. res.*, *submitted*, 2003.

Saathoff, H., C. Linke, O. Möhler, K.H. Naumann, M. Schnaiter, W. Schöck, R. Wagner, and U. Schurath, Influence of coatings on structure and optics of soot aerosol, in *IGAC Conference 2002*, Crete, Greece, http://imk-aida.fzk.de/abstract/, 2002.

Schütz, L., Long range transport of desert dust with special emphasis on the Sahara, in *Aerosols: Anthropogenic and natural sources and transport*, edited by T. Kniep, and P. Lioy, Annals of the New York Academy of Science, 1980.

Seinfeld, J.H., and S. Pandis, *Atmospheric Chemistry and Physics*, 429 pp., John Wiley and Sons, New York, 1998.

Shi, Z., L. Shao, T.P. Jones, A.G. Whittaker, S. Lu, K.A. Berube, T. He, and R.J. Richards, Characterization of airborne individual particles collected in an urban area, a satellite city and clean air area in Beijing, 2001, *Atmospheric Environment*, *37*, 4097-4108, 2003.

Smith, M.H., and C.D. O'Dowd, Observations of accumulation mode aerosol composition and soot carbon concentrations by means of the high-temperature volatility technique, *Journal of Geophysical Research*, *101* (D14), 19583-19591, 1996.

Sokolik, I.N., and O.B. Toon, Incorporation of mineralogical composition into models of the radiative properties of mineral aerosol from UV to IR wavelengths, *Journal of Geophysical Research*, *104*, 9423-9444, 1999.

Streets, D.G., T.C. Bond, G.R. Carmichael, S.D. Fernandes, Q. Fu, D. He, Z. Klimont, S.M. Nelson, N.Y. Tsai, M.Q. Wang, J.H. Woo, and K.F. Yarber, An inventory of gaseous and primary aerosol emissions in Asia in the year 2000, *Journal of Geophysical Research*, 2003.

Tang, Y., and e. al., Three-dimensional studies of aerosol ions and their size-distribution in East Asia during Spring 2001, *Journal of Geophysical Research*, 2003.

Uno, I., G.R. Carmichael, D. Streets, S. Satake, T. Takemura, J.-H. Woo, M. Uematsu, and S. Ohta, Analysis of surface black carbon concentrations during ACE-Asia using a regional-scale aerosol model, *Journal of Geophysical Research*, *108* (D23), 2003.

Wang, H.C., and W. John, Characteristics of the Berner impactor for sampling inorganic ions, *Aerosol Science and Technology*, *8*, 157-172, 1988.

Weber, R.J., S. Lee, G. Chen, B. Wang, V.N. Kapustin, K. Moore, A.D. Clarke, L. Mauldin, E. Kosciuch, C. Cantrell, F. Eisele, D. Thornton, A.R. Bandy, G.W. Sachse, and H.E. Fuelberg, New Particle Formation in Anthropogenic Plumes Advecting from Asia observed during TRACE-P, *Journal of Geophysical Research*, 2003.

Weber, R.J., D. Orsini, Y. Duan, Y.N. Lee, P. Klotz, and F.J. Brechtel, A particle-into-liquid collector for rapid measuremnts of aerosol chemical composition, *Aerosol Science and Technology*, *35*, 718-727, 2001.

Woodward, S., Modeling the atmospheric life cycle and radiative impact of mineral dust in the Hadley Centre climate model, *Journal of Geophysical Research*, *106* (D16), 18155-18166, 2001.

LIST OF FIGURES

decrease again by over an order of magnitude while sizes near 2 μm decrease by a factor of 2 to 3 and the soot near 0.2 μm decrease by a factor of 4 or so.

6. Plots showing effectiveness of our dust distribution at extracting dust tail from soot in refractory accumulation mode (flyash cases removed). Top shows plot of $V_{ref<75}$ vs. PSAP sub-μ absorption color coded by dust concentrations. Bottom - same plot for $V_{ref<75\ -Dust}$ after dust subtraction clearly collapses data down to relation for soot dominated data (blue).

7. "Signature" plot of accumulation mode refractory soot volume with dust tail removed vs. total aerosol light absorption. a) TRACE-P and ACE-Asia data (triangles) – Note the strong linear relation for TRACE-P and most of ACE-Asia where absorption is dominated by refractory soot mode. Deviations above this relationship represent occasional addition of sub-μ non-absorbing aerosol expected to be flyash (eg. $SiO_2$) in Yellow Sea rarely present on TRACE and deviations to higher total absorption below reflect coarse particle absorption from dust. Coarse aerosol volumes greater than 200 $\mu m^2 cm^{-3}$ are highlighted as solid dots to illustrate the role of dust upon total absorption (see text).

8. Plot of light scattering calculated from the OPC size-distributions against measured scattering for scattering angles "seen" by nephelometer for 7-170° for all data (Flight 13 higlighted). Note that data falls on 1:1 line when scattering is dominated by sub-μ aerosol but at higher scattering values dominated by dust the calculated values are about 10% larger than measured.

9. Asymptotic behavior for plot of coarse particle volume absorption efficiency (VAE) vs. coarse particle OES volume with Flight 13 flight legs highlighted. Asymptote constrains value of dust refractive indices between k = 0.0007 and 0.0005. A) VAE as measured; B) VAE calculated based for k=0.0006 and impactor transmission that includes some accumulation mode soot in coarse mode; C) PSAP sub-μ absorption vs. coarse absorption – note net positive slope of data D) PSAP sub-μ absorption vs. coarse absorption subtracting model dust absorption – note more compact data cloud with many points corrected to near zero absorption but slope remains. (see text)

10. (a) Typical distributions of representative refractory soot (assumed same as BC-blue) and dust (green). (b) size-dependent MSE (dashed) and MAE (solid) properties modeled for BC and dust based upon refractive indices discussed in text. (c) representative absorption distributions for BC and dust (d) Size dependent ϖ for dust and BC shown in (a) and a mix of BC with non-absorbing volatiles similar to ACE-Asia aerosol.

11. (a) Relationships between absorption of BC, EC and refractory volume over sample periods for EC of about 30min. Slopes and correlations are indicated for total and sub-μ PSAP measurements. Solid circles indicate absorption influenced by elevated dust concentration above about 500 μg $m^{-3}$. The MAE values from the slope of the regression from 6.1 $m^2g^{-1}$ (sub-μ) to 8.1 $m^2g^{-1}$ for total aerosol. (b) $V_{ref<75\text{-}Dust}$ vs. EC showing similar correlation coefficient as relationship in (a). (c) Correlation between PSAP absorption and refractory OPC volumes are much higher with $R^2$ of 0.75 and slope value is VAE. The combined a-b-c plots demonstrate that the EC measurement has the largest uncertainty associated with it.

12. (a) Plots of the refractory soot fraction [$\mathbf{V_{ref<75\text{-}Dust}}$ / $\mathbf{V_{tot<75\text{-}Dust}}$] of the accumulation mode volume and the ϖ for the sub-μ mode as a function of coarse dust volume for all horizontal legs below 2 km during the entire ACE-Asia experiment obtained every 90s. As the fraction of refractory soot increases (less volatiles) less scattering is contributed by volatiles due to their uptake onto coarse aerosol. This result in lower values for sub-μ ϖ. Bin averaged values are highlighted for both parameters. When the bin average co-albedo (1-ϖ) is plotted against $\mathbf{V_{ref<75\text{-}Dust}}$ / $\mathbf{V_{tot<75\text{-}Dust}}$ **(see insert)** this relation has a slope of 0.68 and an $R^2$ of 0.94 and indicating that the mix of BC to volatiles in the sub-μ mode and its optical properties are strongly influenced by the dust. (see text).
(b) The lower panel includes corresponding bin averaged values of PILS combined sulfate, nitrate and ammonium mass; the total volatile volume estimated to be "seen" by PILS below 1.2 μm and the total volume below 0.75μ OES diameter as a function of the coarse dust volume. Peak values occur at coarse volume concentrations characteristic of urban pollution and drop at higher concentrations of dust consistent with loss to the dust surface (see text).

13. Comparison of CTM model results for BC with results for CFORS BC emissions for TRACE-P and ACE-Asia. (a) Plot of PSAP absorption vs. $BC_{model}$ for TRACE-P data color stratified by ratio of measured to model CO concentrations. Average MAE values for both groupings are indicated. (b) PSAP absorption vs. $BC_{model}$ for ACE-Asia showing a branched relationship. High model biomass and high model fossil fuel CO values are shaded and show up on different branches. (c) $V_{ref<75\ -Dust}$ vs. $BC_{model}$ for same data as (b) confirming that sub-μ refractory $V_{ref<75\ -Dust}$ reveals the same behavior for these highlighted cases. (d) Plot of $V_{ref<75\ -Dust}$ vs. PSAP absorption showing that both data groups have the same slope (ie. same MAE values) and confirming that differences are not related to soot optical properties but to model performance. (see text for details).

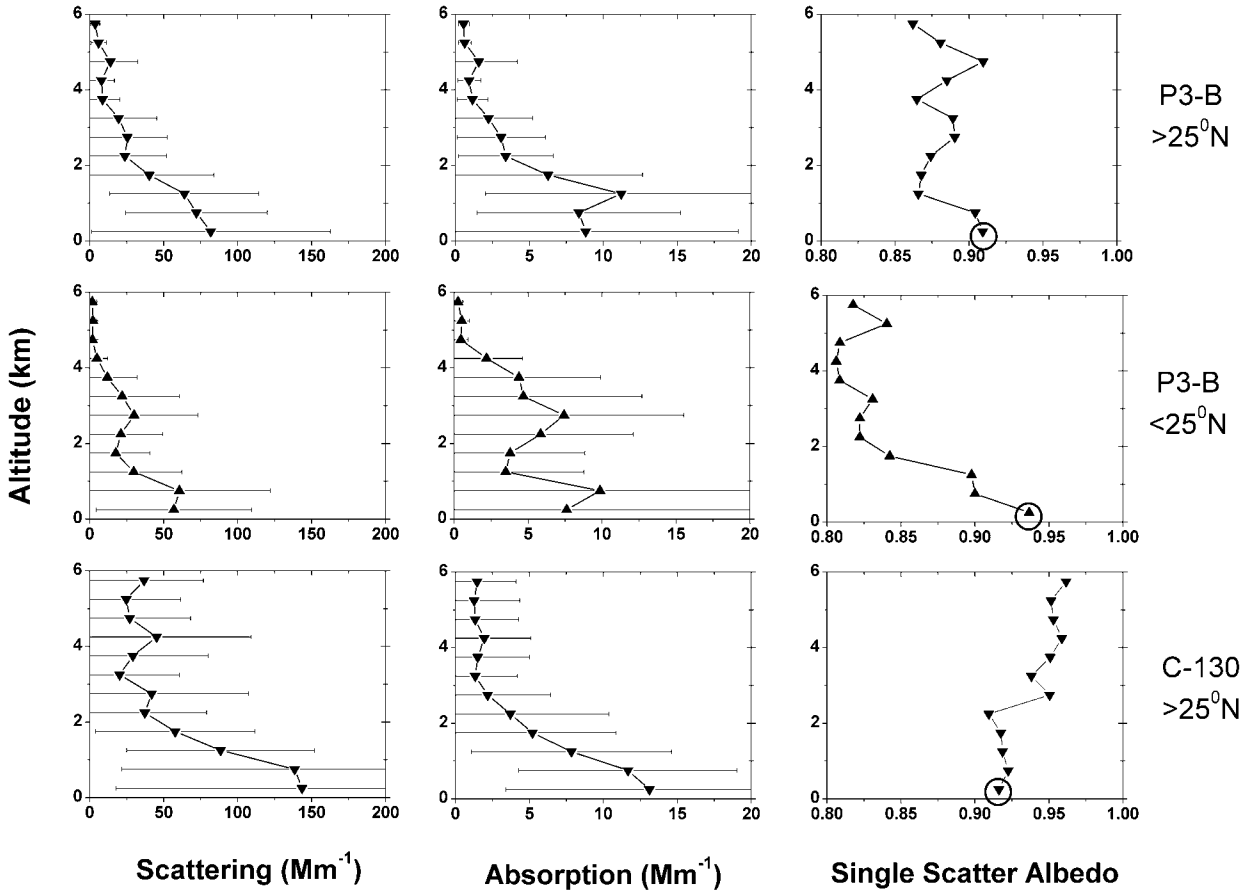
Altitude (km)
Scattering (Mm-1)
Absorption (Mm-1)
Single Scatter Albedo
P3-B
>25°N
P3-B
<25°N
C-130
>25°N

Figure 1

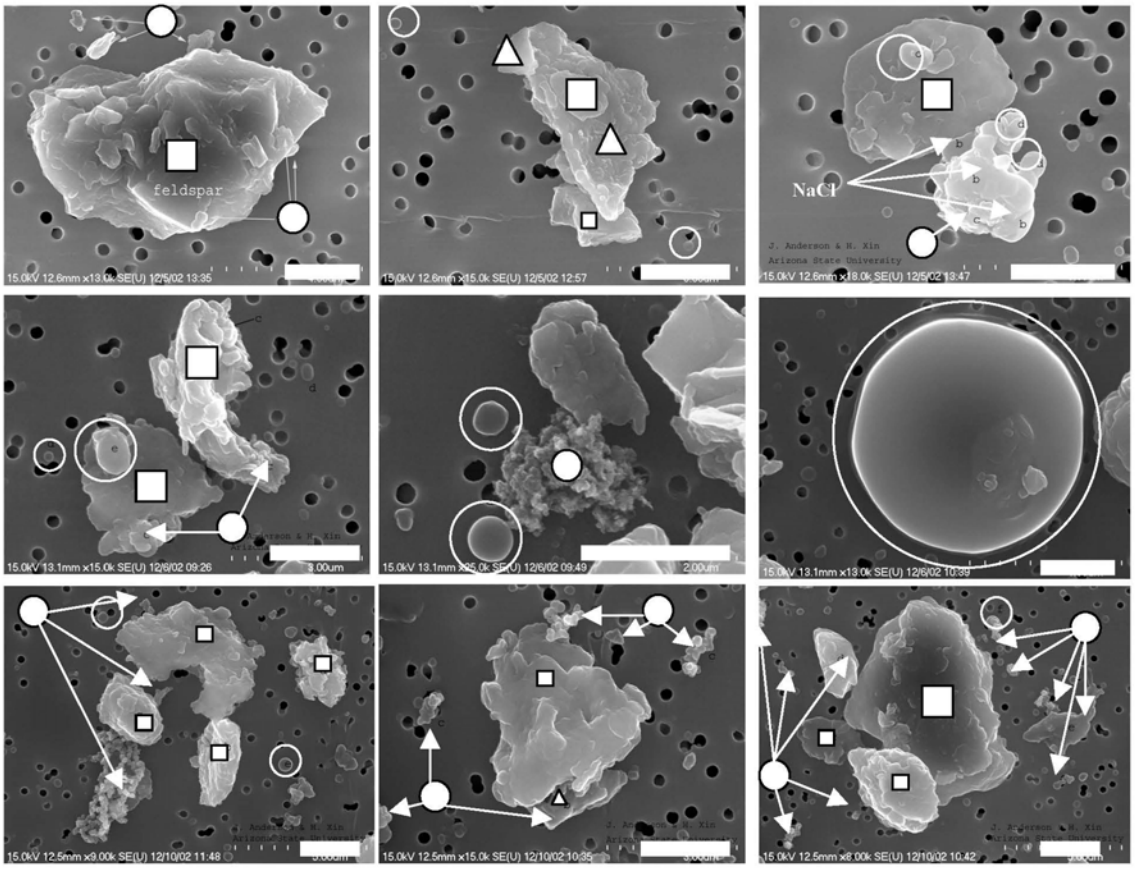


Figure 2

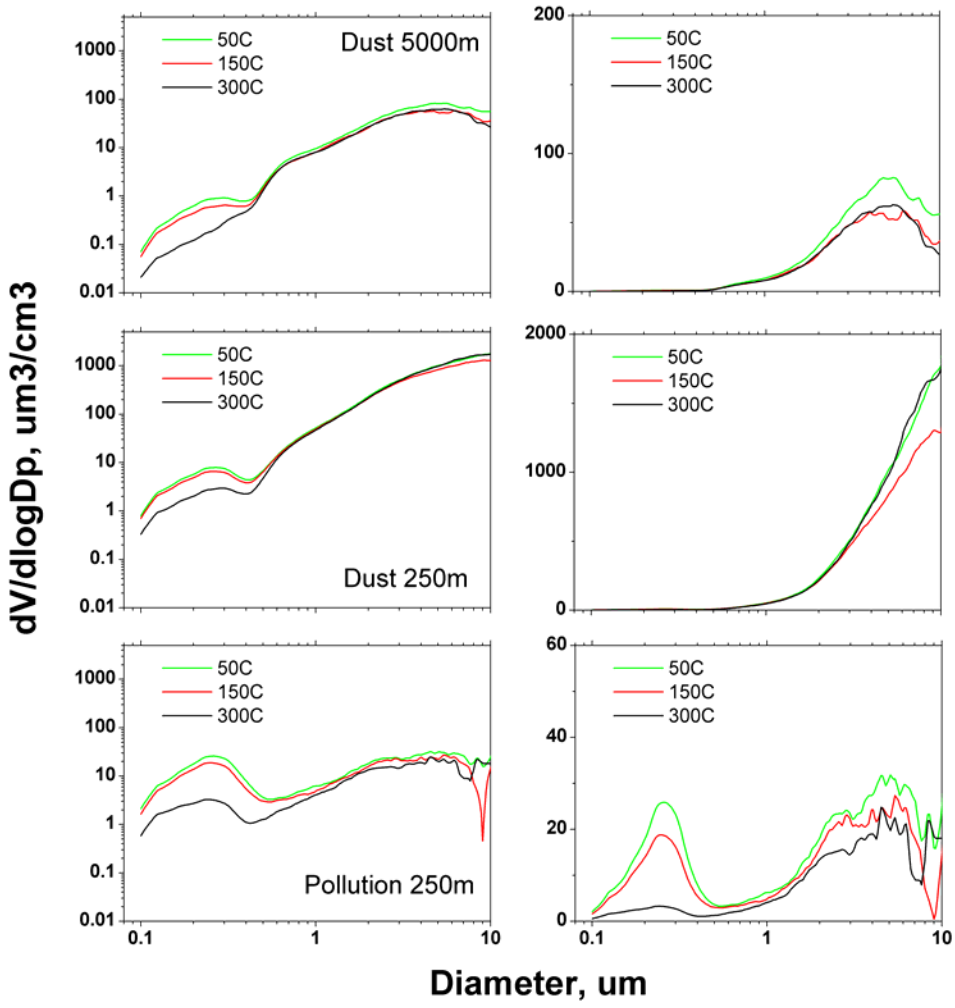
dV/dlogDp, um3/cm3
Diameter, um
Dust 5000m
Dust 250m
Pollution 250m
50C
150C
300C

Figure 3

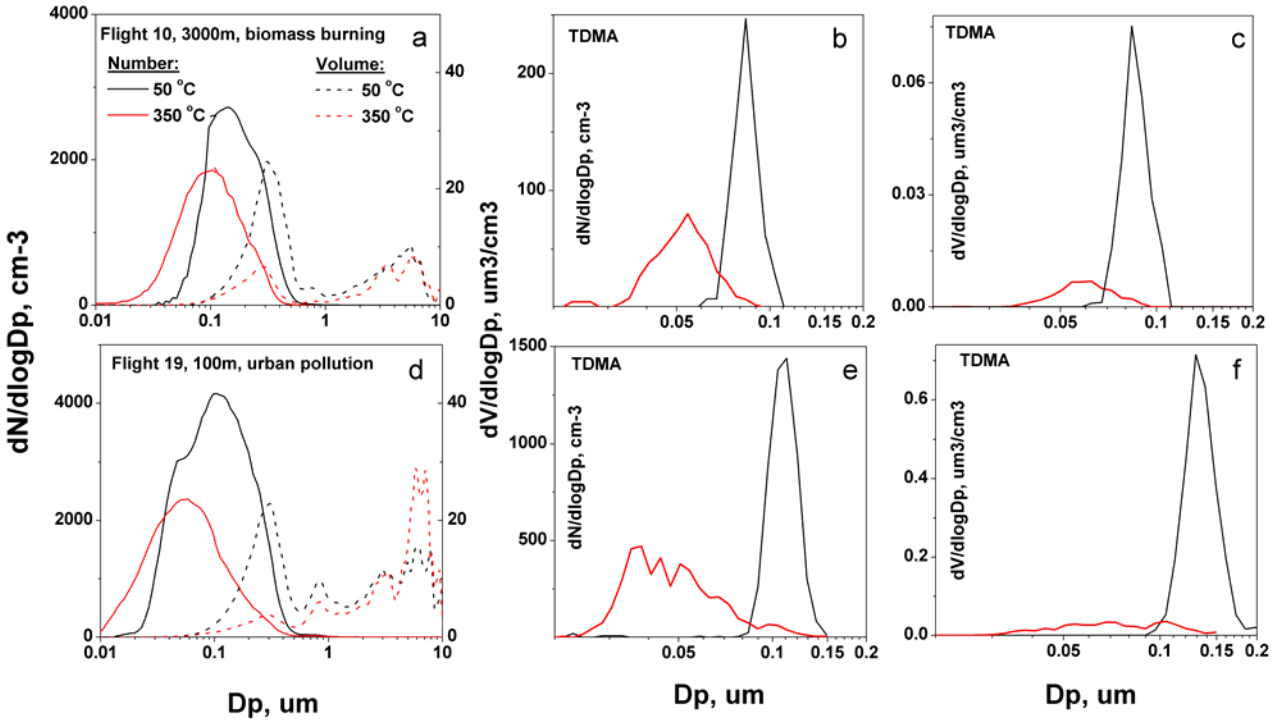
Flight 10, 3000m, biomass burning
a
Number:
Volume:
50 °C
350 °C
50 °C
350 °C
Flight 19, 100m, urban pollution
d
TDMA
b
TDMA
c
TDMA
e
TDMA
f
dN/dlogDp, cm-3
dV/dlogDp, um3/cm3
Dp, um

Figure 4

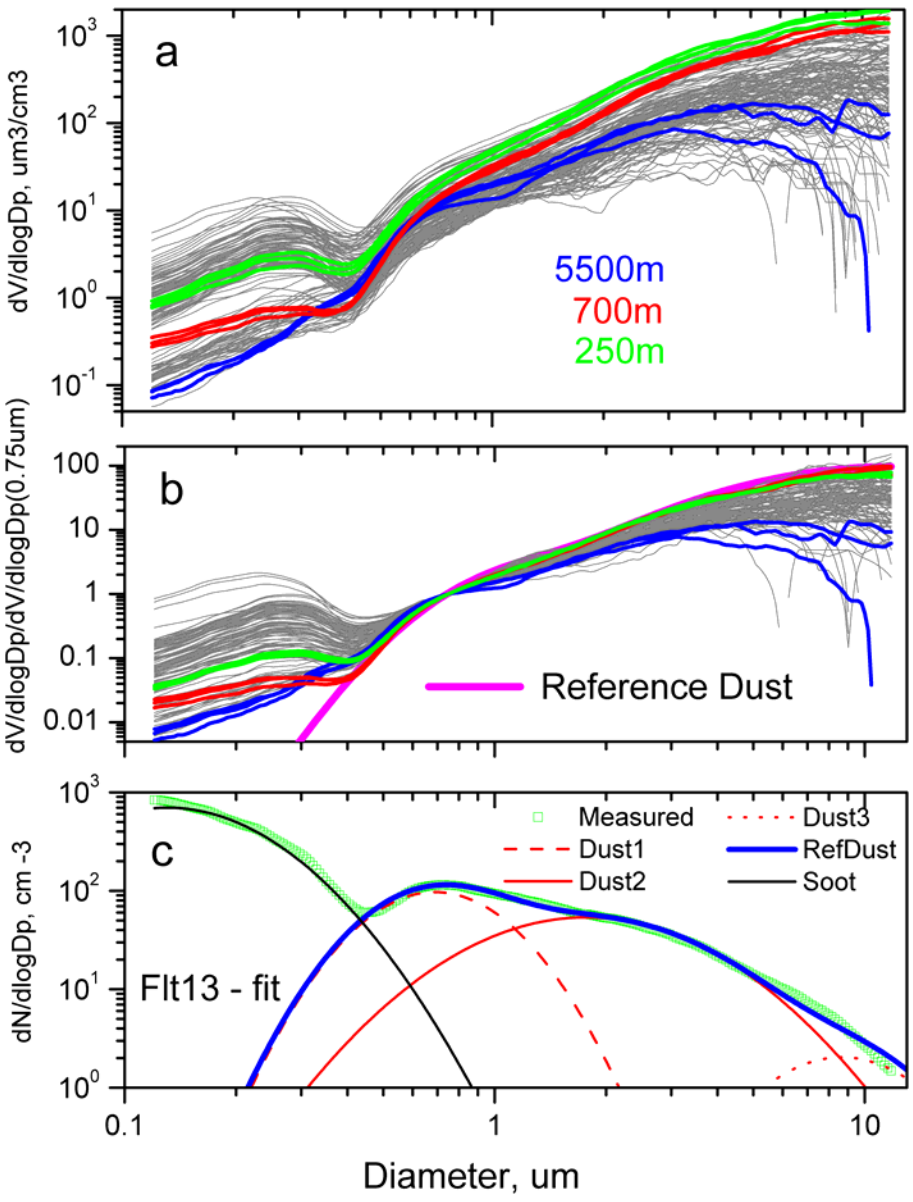
a
dV/dlogDp, um3/cm3
5500m
700m
250m
b
dV/dlogDp/dV/dlogDp(0.75um)
Reference Dust
c
dN/dlogDp, cm -3
Measured
Dust3
Dust1
RefDust
Dust2
Soot
Flt13 - fit
Diameter, um

Figure 5

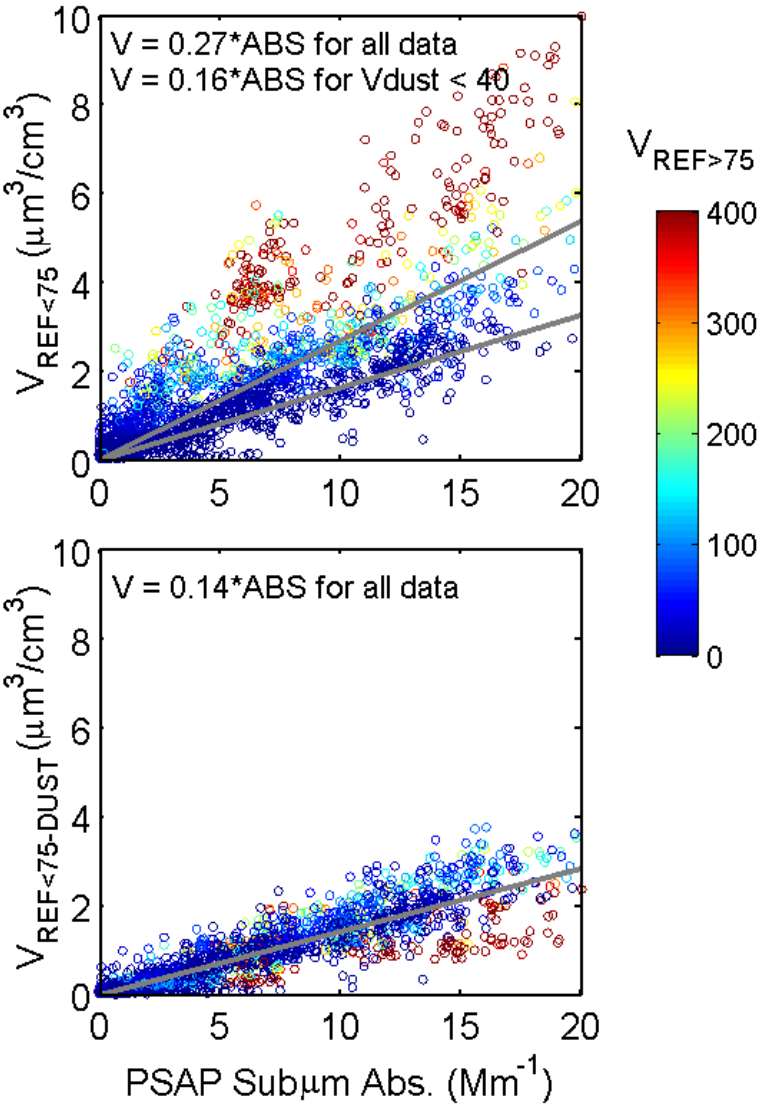
V = 0.27*ABS for all data
V = 0.16*ABS for Vdust < 40
V = 0.14*ABS for all data
V_REF<75 (μm^3/cm^3)
V_REF<75-DUST (μm^3/cm^3)
PSAP Subμm Abs. (Mm^-1)
V_REF>75
400
300
200
100
0
0
2
4
6
8
10
0
5
10
15
20

Figure 6

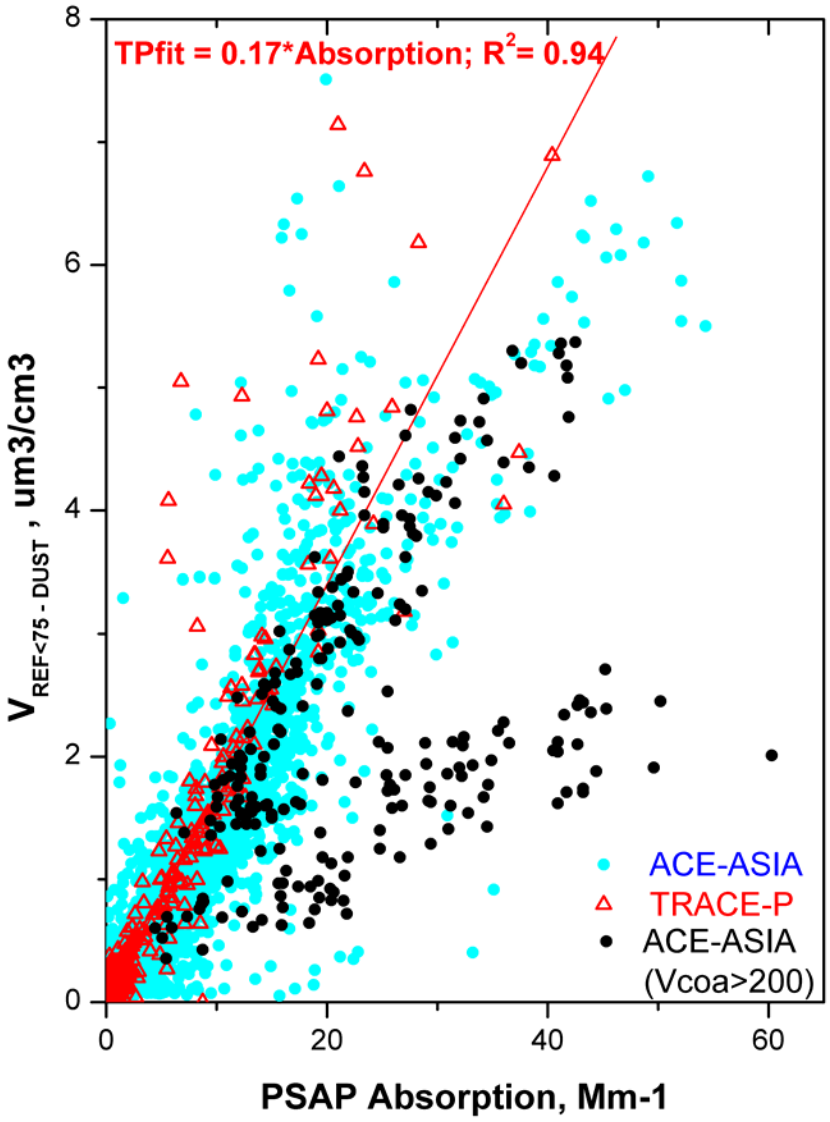
TPfit = 0.17*Absorption; R2= 0.94
VREF<75 - DUST , um3/cm3
PSAP Absorption, Mm-1
ACE-ASIA
TRACE-P
ACE-ASIA
(Vcoa>200)
0
2
4
6
8
0
20
40
60

Figure 7

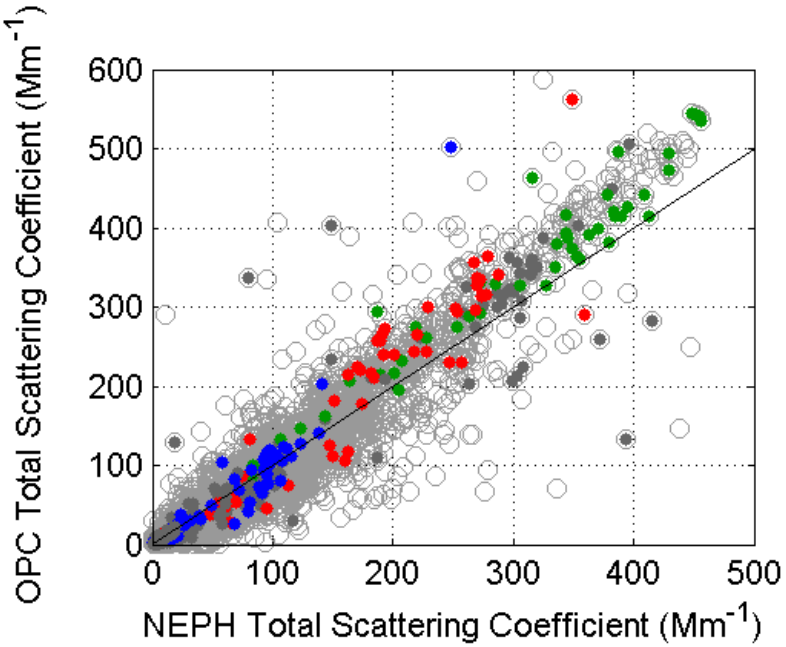
OPC Total Scattering Coefficient (Mm$^{-1}$)
NEPH Total Scattering Coefficient (Mm$^{-1}$)
0
100
200
300
400
500
600

Figure 8

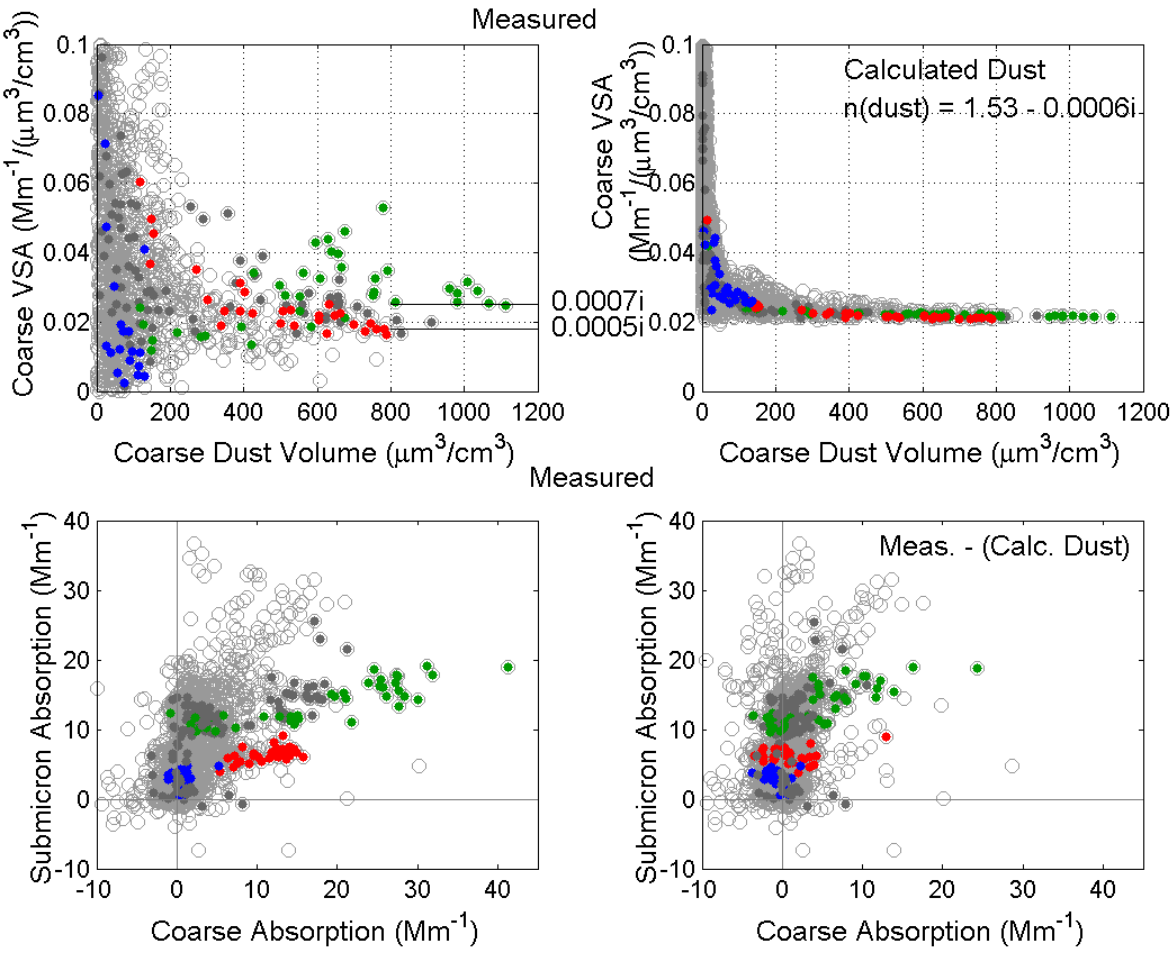
Measured
Coarse VSA (Mm-1/(μm3/cm3))
Coarse Dust Volume (μm3/cm3)
0.0007i
0.0005i
Calculated Dust
n(dust) = 1.53 - 0.0006i
Measured
Submicron Absorption (Mm-1)
Coarse Absorption (Mm-1)
Meas. - (Calc. Dust)

Figure 9

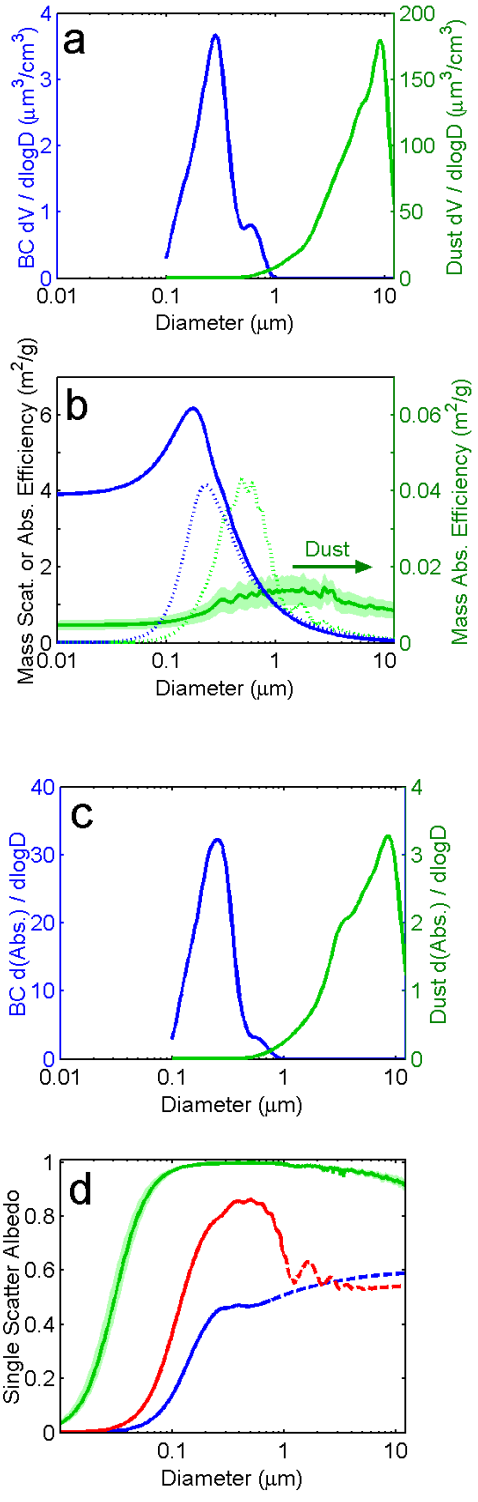
a
BC dV / dlogD (μm3/cm3)
Dust dV / dlogD (μm3/cm3)
Diameter (μm)
b
Mass Scat. or Abs. Efficiency (m2/g)
Mass Abs. Efficiency (m2/g)
Dust
Diameter (μm)
c
BC d(Abs.) / dlogD
Dust d(Abs.) / dlogD
Diameter (μm)
d
Single Scatter Albedo
Diameter (μm)

Figure 10

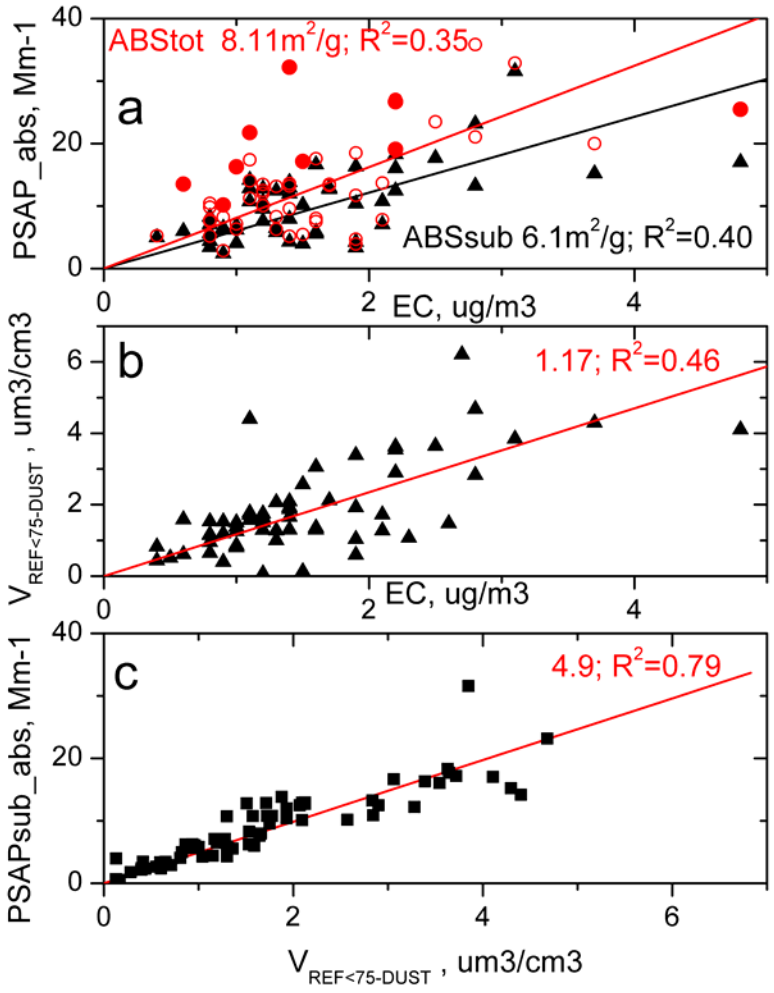
ABStot 8.11m²/g; R²=0.35
a
ABSsub 6.1m²/g; R²=0.40
PSAP_abs, Mm-1
EC, ug/m3
b
1.17; R²=0.46
V REF<75-DUST , um3/cm3
EC, ug/m3
c
4.9; R²=0.79
PSAPsub_abs, Mm-1
V REF<75-DUST , um3/cm3

Figure 11

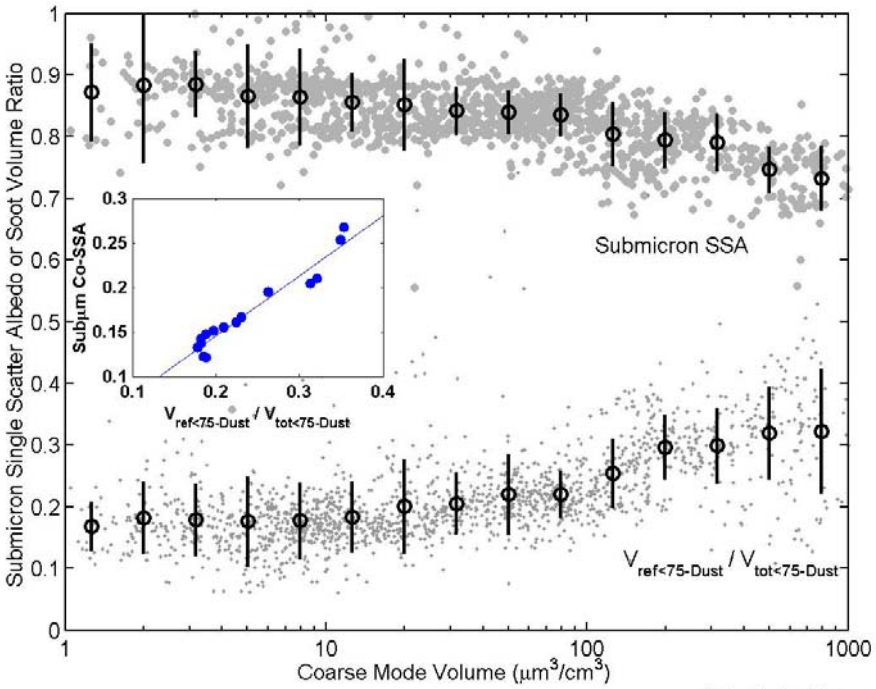
Submicron Single Scatter Albedo or Soot Volume Ratio
Coarse Mode Volume (μm³/cm³)
Submicron SSA
V ref<75-Dust / V tot<75-Dust
Subμm Co-SSA
V ref<75-Dust / V tot<75-Dust

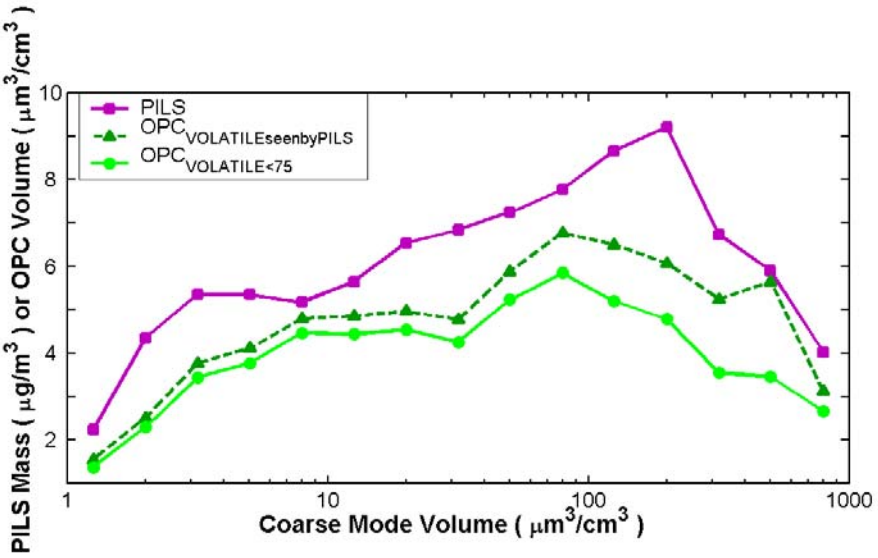
PILS
OPC VOLATILEseenbyPILS
OPC VOLATILE<75
PILS Mass ( μg/m³ ) or OPC Volume ( μm³/cm³ )
Coarse Mode Volume ( μm³/cm³ )

Figure 12

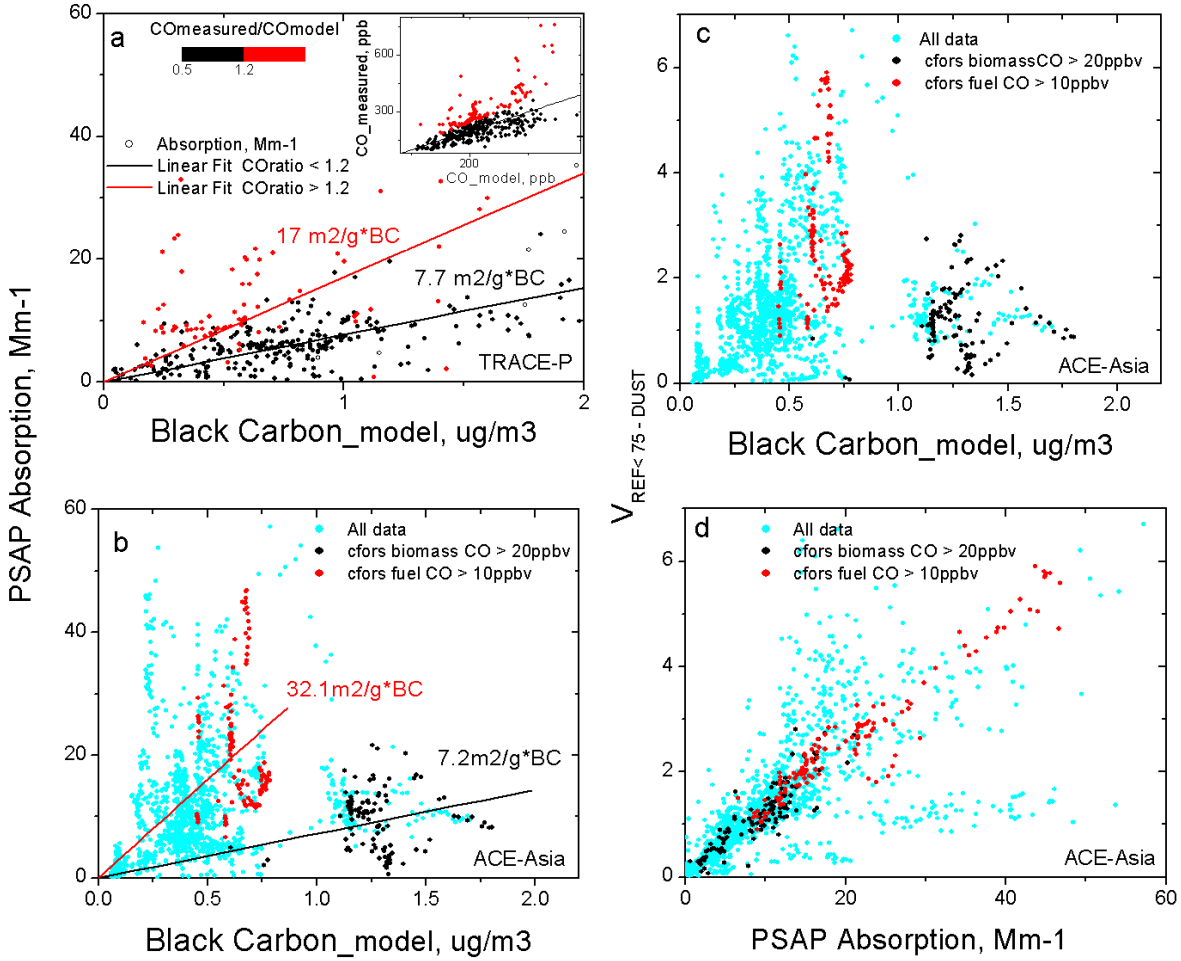
a
COmeasured/COmodel
0.5
1.2
Absorption, Mm-1
Linear Fit COratio < 1.2
Linear Fit COratio > 1.2
17 m2/g*BC
7.7 m2/g*BC
TRACE-P
CO_measured, ppb
CO_model, ppb
PSAP Absorption, Mm-1
Black Carbon_model, ug/m3
b
All data
cfors biomass CO > 20ppbv
cfors fuel CO > 10ppbv
32.1m2/g*BC
7.2m2/g*BC
ACE-Asia
Black Carbon_model, ug/m3
c
All data
cfors biomassCO > 20ppbv
cfors fuel CO > 10ppbv
ACE-Asia
Black Carbon_model, ug/m3
V REF< 75 - DUST
d
All data
cfors biomass CO > 20ppbv
cfors fuel CO > 10ppbv
ACE-Asia
PSAP Absorption, Mm-1

Figure 13